

Bandgap modulation of graphene oxide and its application in
the photocatalytic deposition of metallic nanoparticles

By

Sina Abdolhosseinzadeh

Submitted to the Graduate School of Engineering and Natural Sciences
in partial fulfillment of the requirements for the degree of
Master of Science

Sabanci University

July 2017

Bandgap modulation of graphene oxide and its application in
the photocatalytic deposition of metallic nanoparticles

APPROVED BY:

Assoc. Prof. Dr. Selmiye Alkan Gürsel
(Thesis Supervisor)



.....

Assoc. Prof. Dr. Önder Metin



.....

Assist. Prof. Dr. Alp Yürüm



.....

DATE OF APPROVAL: 31/07/2017

©2017 by Sina Abdolhosseinzadeh

ALL RIGHTS RESERVED

Bandgap modulation of graphene oxide and its application in the photocatalytic deposition of metallic nanoparticles

Sina Abdolhosseinzadeh

Materials Science and Nano-Engineering, MSc Thesis, 2017

Supervisor: Assoc. Prof. Selmiye Alkan Gürsel

Keywords: Partially reduced graphene oxide, Platinum nanoparticles, Palladium, Gold, Silver, Metallic nanoparticles, Nanoclusters, Photocatalytic deposition, Partial reduction, Bandgap modulation.

Abstract: In this project, a novel photocatalytic system for deposition of nano- and sub nano-sized metallic (platinum, palladium, gold and silver) particles on reduced graphene oxide has been developed. Partially reduced graphene oxide, a bandgap engineered form of graphene, has been used as the deposition platform and its chemical stability and bandgap modulation process has been discussed in great details. For the partial reduction, graphene oxide has been treated with highly concentrated sodium hydroxide solution and the reduction process has been continued (and monitored) until obtaining a stable product.

We have also shown that graphene oxide which also exhibits semiconducting properties, isn't a suitable photocatalyst materials mainly because of its chemical instability and considerable photocorrosion. An innovative reactor for pulsed UV illumination and continuous treatment of the reaction suspensions has been designed and fabricated during this thesis work which enables us to have precise control on the number of photoexcited electrons and consequently on the photodeposition of the metallic nanoparticles.

Grafen oksitin bant-boşluk modülasyonu ve metalik nanopartiküllerin fotokatalitik oturtması

Sina Abdolhosseinzadeh

Malzeme Bilimi ve Mühendisliği, MSc Tezi, 2017 Tez

Danışmanı: Doç. Dr. Selmiye Alkan Gürsel

Anahtar kelimeler: Kısmen indirgenmiş grafen oksit, Platin nanopartiküller, Metalik nanopartiküller, Nanokütanlar, Fotokatalitik Depozisyon, Kısmi indirgenme, Bandgap modülasyonu.

Özet:

Bu projede, RGO üzerinde nano boyutlu metalik (platin, palladyum, altın ve gümüş) partiküllerinin oturtması amacıyla, yeni bir fotokatalitik sistem geliştirildi. Kısmen indirgenmiş grafen oksit (PRGO), bandgapla tasarlanmış bir grafenin formu, çökeltme platformu olarak kullanılmıştır ve onun kimyasal dayanıklılığı ve band açma modülasyonu prosesinin üzerinde çok basit bahs edildi. Kısmi indirgeme için, grafen oksiti yüksek derecede konsantre bir sodyum hidroksit çözeltisi ile işleme tabi tutuldu ve indirgeme işlemi, istikrarlı bir ürün elde edilinceye kadar sürdürüldü (ve izlendi).

Aynı zamanda, yarı iletkenlik özellikleri gösteren grafen oksitin, kimyasal istikrarsızlığı ve fotokorozyonu nedeniyle uygun bir fotokatalist materyali olmadığını da göstermiş olduk. Darbeli UV aydınlatması ve reaksiyon süspansiyonlarının sürekli arıtılması için yenilikçi bir reaktör tasarlandı ve fotoğlanılan elektronların sayısını ve sonuç olarak metalik nanopartiküllerin foto-çökmesini hassas bir şekilde kontrol etmemizi sağlayan bu tez çalışması sırasında imal edildi.

Acknowledgment

I would like to gracefully thank my supervisor, Professor Selmiye Alkan Gürsel, who has kindly, generously and very strongly supported me during this research.

I also thank my thesis defense jury members who have reviewed this dissertation with meticulous consideration.

Finally, yet importantly, I would like to appreciate the great support of my dear wife and my lovely parents who I owe them my life and all my achievements.

Sina Abdolhosseinzadeh

I would like to dedicate this thesis to my wife and my parents.

Table of Contents

Abstract	IV
Özet	V
Acknowledgement	VI
Table of Contents	VIII
List of Figures	IX
1. Introduction	1
1.1. Graphene-noble metals composites.....	2
1.2. Graphene: Properties and Synthesis methods.....	3
1.3. Synthesis of graphene-noble metals composites.....	8
1.4. Partially reduced graphene oxide: Synthesis and bandgap modulation.....	10
2. Objectives of this thesis	15
3. Materials and methods.....	17
3.1. Synthetic procedures.....	18
3.1.1. Synthesis of PRGO.....	18
3.1.2. Photocatalytic deposition of platinum on PRGO.....	18
3.1.3. Photocatalytic deposition of palladium on PRGO.....	19
3.1.4. Photocatalytic deposition of gold on PRGO.....	19
3.1.5. Photocatalytic deposition of silver on PRGO.....	20
3.2. Reactor design.....	20
3.3. Instrumentation	21
4. Results and discussions.....	23
4.1. Partial reduction of GO and bandgap modulation.....	24
4.2. UV-vis spectroscopy and bandgap calculations.....	24
4.3. Raman spectroscopy.....	25
4.4. X-ray photoelectron spectroscopy for monitoring the reduction....	26
4.5. X-ray photoelectron spectroscopy for photostability studies.....	30
4.6. X-ray diffraction analysis.....	32
4.7. TEM studies of Pt deposition.....	33
4.8. X-ray photoelectron spectroscopy for photocatalytic reduction studies.....	35
5. Conclusions	37
References	39

List of Figures

Figure 1. Consecutive stages of graphite exfoliation via scotch tape method.....	4
Figure 2. Three-roll mill method for exfoliation of graphite by exertion of mechanical forces (taken from reference [23]).....	5
Figure 3. a) Sonication-assisted exfoliation of graphite (taken from ref. [29]); b) Exfoliation of graphite by means of a high-shear mixer (taken from ref. [25]).....	6
Figure 4. Picturing two different viewpoints against reduced graphene oxide. Considering the car in (a) as pristine graphene, some researchers consider the reduced graphene oxide as the damaged car shown in (b) but the car in (c) can also represent the reduced graphene oxide because although it is not suitable for routine applications but on snow, it is preferred to the car shown in (a).....	7
Figure 5. Schematic illustration of (a) NEG-decorated (functionalized) graphene; (b) in dark situation (NEGs are off); (c) NEG-decorated (functionalized) graphene under UV illumination where growth of Pt nanoparticles has started. The blue and yellow colored atoms have sp^2 and sp^3 hybridizations, respectively.....	10
Figure 6. The dependence of the position of the valence band maximum (VBM) and conduction band minimum (CBM) of GO sheets with the variation of their oxygenation content (taken from ref. [56]).....	12
Figure 7. Schematic and real images of the photocatalytic deposition reactor; (a) the main components of the reactor; (b) quartz tubes with different exposure lengths (cm) to control the duration of UV illumination (duration of the pulses); (c) cross-sectional view of the deposition compartment demonstrating the arrangement of the UV lamps and the quartz tube; (d) real image of the reactor.....	21
Figure 8. (a) Normalized UV-Vis spectra of GO and PRGO2-10 (an offset to the absorbance has been applied to make the peak shift more visible); Application of Tauc plot for optical band gap calculation of (b) GO; (c) PRGO2; (d) PRGO4; (e) PRGO6; (f) PRGO8; (g) PRGO10.	25
Figure 9. Normalized Raman spectra of GO and PRGO2-10 excited with a 532 nm laser source.....	26

Figure 10. Deconvoluted XPS C _{1s} peak of (a) GO, (b) PRGO2, (c) PRGO4, (d) PRGO6, (e) PRGO8, and (f) PRGO10 showing gradual elimination of OFGs (assignment of the colors is similar from a-f).....	28
Figure 11. Evolution of optical bandgap, alteration of I _D to I _G ratio (I _D /I _G) of the Raman spectrum's D and G bands, and concentration changes of hydroxyl, epoxide, carbonyl and carboxyl groups with respect to the reduction time (treatment with NaOH) in a single graph for comparing the trends.....	29
Figure 12. XPS analysis for monitoring the photostability of (a) GO and (b) PRGO8 after 4, 8 and 12 h exposure to UV light (for instance, GO-UV8 corresponds to a sample of GO which has been exposed to UV light for 8 hours).....	31
Figure 13. Normalized XRD patterns of graphite, GO, PRGO8 and PtRGO120-20%.....	32
Figure 14. Normalized XRD patterns of PdRGO, PtRGO120-60%, PtRGO120-20%, AgRGO and AuRGO	33
Figure 15. (a) TEM image of PtRGO120-20% showing the uniform distribution of the Pt nanoclusters; (b) TEM image and corresponding size histogram (inset) of the PtRGO120-20% showing the morphology of the Pt nanoclusters; (c) TEM image of PtRGO60-100% showing the uniform distribution of the Pt nanoparticles; (d) TEM image and corresponding size histogram (inset) of the PtRGO60-100% showing the morphology of the Pt nanoparticles; (e) TEM image of a composite which has been produced at the same conditions as PtRGO60-100% but with replacing the PRGO8 with GO.....	34
Figure 16. (a) XPS survey spectrum before treatment with ascorbic acid; (b) XPS Pt _{4f} peak of the PtPRGO120-20% sample; (c) XPS C _{1s} peak of PRGO8 and PtRGO120-20% which shows the removal of the majority of the OFGs.....	36

Introduction

1. Introduction

1.1. Graphene-noble metals composites

Metallic nanoparticles, especially noble metals such as platinum, palladium, gold, silver etc. have exhibited great performance in numerous fields of science and technology such as in catalysis, electronics, sensors, and medicine [1]. However, due to their high costs and limited resources, several attempts have been made to increase their specific performance (yield per gram of the noble metal). The reduction of the size [2] and the increase in active surface area [3] of the particles are two most important and straight forward strategies which have already become matured and further improvement of the specific performance via these approaches is very hard or almost impossible.

The incorporation of other nanomaterials with large surface areas and considerable electrical and catalytic properties to noble metals is another approach which has shown great promise for enhancement of the specific performance. Carbonaceous materials such as activated carbon [4], carbon black [5], carbon nanotubes [6], fluorenes [7] and graphene [8] are some of the most widely studied materials for this purpose. Although composites of noble metals with nano-sized carbon-based substrates such as carbon nanotubes (single- and multi-wall) and fluorenes have exhibited significant enhancements in their catalytic, electrochemical and electrical performance but the high costs and complex production procedures of these supports have limited their applications [9]. On the other hand, the theoretical surface area and catalytic activity of the cheap and commercially available members of this family (carbonaceous materials) aren't comparable with those of the nanometer sized members. However, the youngest member of this group, graphene, can potentially address both of the aforementioned drawbacks.

Like most other nanomaterials, graphene can also be produced by both bottom-up [10] and top-down [11] approaches. Fortunately, graphite as the parent material for the production of graphene through top-down approaches, is abundantly available for very low-cost which is the main advantage of graphene over other carbon-based nanomaterials. The other very important advantage of graphene with regard to other carbon-based supports is that it can be easily

functionalized and its chemical and physical properties are tunable by the degree of its functionalization. This specific trait of graphene enables us to tune its properties according to the requirements of desired application [12].

To date, numerous methods have been developed for the synthesis of graphene but virtually no two products, produced by any of these methods are identical! In fact, the physical and chemical properties of the produced graphene are extremely dependent on the production method. This is mainly due to the fact that several parameters such as sheet size [13], the configuration of atoms at the edges (zigzag, armchair, etc.) [14], number of the layers [15], presence of other molecules and atoms (attached covalently or non-covalently) [16] and concentration of the defects (on the basal plane) [17] can drastically affect the physical and chemical properties of the graphene.

1.2. Graphene: Properties and Synthesis methods

Graphene is a single layer of sp^2 hybridized carbon atoms in which the atoms are organized into a honeycomb like lattice [18]. Inside the basal plane, each carbon atom has three strong σ bonds (covalent) with three neighboring atoms and one free electron in its π orbital [19]. The conjugation of these π orbitals and consequently, the formation of delocalized-electron clouds over (and under) a single graphene sheet is responsible for the interesting and unique electronic properties of graphene [20]. Any interruption in this conjugated system, caused by any means such as interactions of other atoms or presence of defects in the basal plane can drastically affect the electronic properties of graphene [17]. The Van der Waals interactions of the same π -orbital electrons are responsible for the integrity of the graphite's structure and hence, the weakening of these forces and separation (exfoliation) of the stacked graphene layers (of graphite) is the main goal in almost all top-down approaches [21].

As mentioned earlier, the abundance of graphite as a starting material for the synthesis of graphene has made it a promising candidate from the commercial point of view and hence, the top-down approaches are of greater interest to the scientific society. Probably, the scotch tape method (Figure 1) which has been utilized by Andre Geim and Konstantin Novoselov in their Nobel prize winning work, is the

most well-known example of the top-down approaches [22]. Although the quality of the graphene produced by this method is very high but the production yield is so low that its application is limited to only lab-scale works. However, from that time on, the concept of exfoliating graphite by the application of mechanical forces has been extensively utilized in several works.

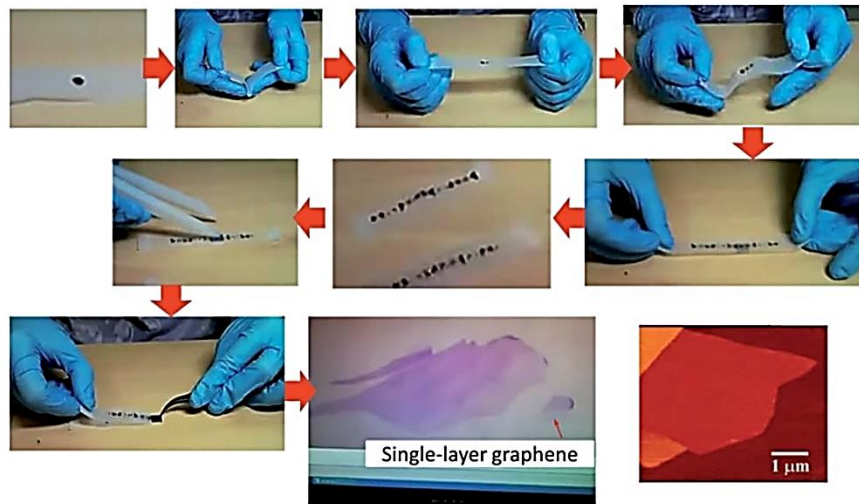


Figure 1. Consecutive stages of graphite exfoliation via scotch tape method.

For instance, inspired by the scotch tape method, Chen et al. have developed a continuous mechanical exfoliation method in which a mixture of graphite and adhesive materials passes through several rolls for numerous times [23]. At the end, a paste of graphene and polymeric materials is obtained. In the next step, by means of organic solvents and heat treatment, the polymeric materials are removed and graphene platelets are obtained. Unfortunately, single layer (and even few layer) graphene is hard to be produced by this method and presence of impurities and low production yield have restricted its application. Several other methods with few modifications have also been developed but none of them has been commercialized [24].

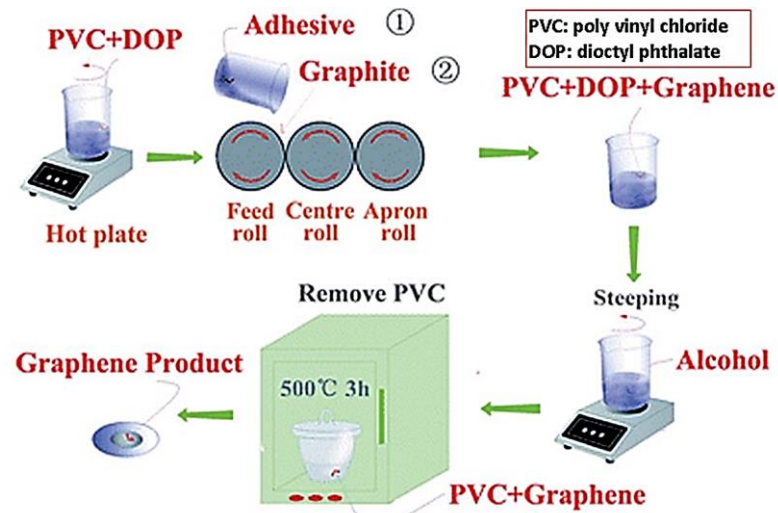


Figure 2. Three-roll mill method for exfoliation of graphite by exertion of mechanical forces (taken from reference [23]).

In another group of the “mechanical exfoliation methods” which have been more successful than the previous group, the mechanical force is applied to graphite layers by means of some special liquid mediums. The proper selection of the medium is the most critical issue in these methods. To make the exfoliation process thermodynamically favorable, the surface tension of the medium should match with the surface energy of the graphene [25]. Based on the theoretical calculations and experimental results, N-Methyl-2-pyrrolidone has been found to be the best medium for this purpose; however, other solvents such as dimethyl sulfoxide and dimethylformamide have also been extensively studied in various works [26]. Ultrasonic waves (with bath- and probe-sonicator) [27] and shear forces inside the dispersion medium (with a high-shear mixer) [25] are two most successful ways of the exertion of the force but the production yield in both cases are far below the minimum requirements of an industrially feasible method. Furthermore, obtaining single layers of graphene requires much longer processing times and the long ultrasonic treatments will have adverse effect on the quality of the produced graphene [28].

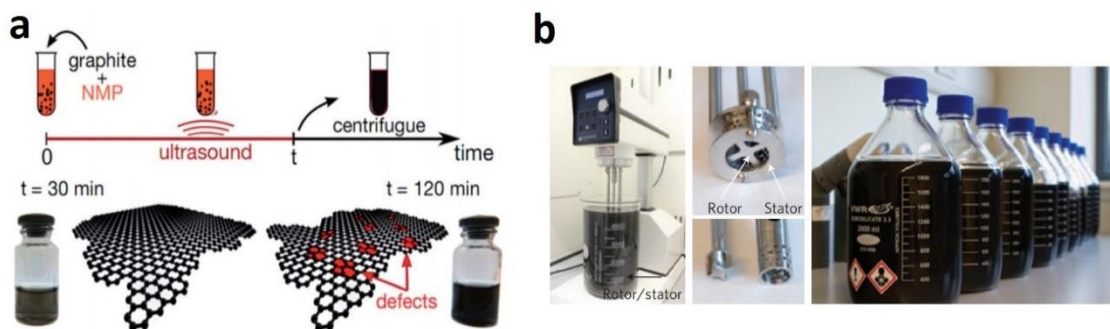


Figure 3. a) Sonication-assisted exfoliation of graphite (taken from ref. [29]); b) Exfoliation of graphite by means of a high-shear mixer (taken from ref. [25]).

Currently, surfactant-assisted (noncovalent functionalization) exfoliation of graphite in water (water-based solvents) seems to be the most promising approach in mechanical exfoliation of graphite and several commercial products have been produced by these methods [30]. When surfactant molecules attach (noncovalently) to the topmost layer of the graphite, they weaken the Van der Waals forces between the layers and by application of a mild force such as ultrasonic waves or shear forces, the layers are peeled off one by one [31]. Ethyl cellulose, sodium dodecyl sulfate and sodium dodecyl benzene sulfonate are some of the most effective surfactants for the liquid-phase exfoliation of the graphite and the quality (e.g. electrical properties) of the produced graphene is so high that they can be used in printed electronics applications [32]. Low production capacity (with low yield) is probably the most important drawback of these methods but virtually there is no other alternative for large scale synthesis of high-quality graphene at the moment.

The other major group of methods for the exfoliation of graphite involves with the covalent functionalization of the graphene. Oxidation-based approaches such as Hummers or Bordie methods utilize harsh oxidative environments to introduce several functional groups (mostly oxygen containing groups) to graphite layers. As a result, the interlayer distance of the graphite sheets increases significantly and the Van der Waals interactions between the layers becomes negligible [21]. Furthermore, when a functional group forms covalent bond with a carbon atom of

the graphene sheet, the hybridization of the carbon atom transforms from sp^2 to sp^3 which also results in the elimination of the Van der Waals interactions. The product of this process is graphite oxide which can be exfoliated to graphene oxide by means of sonication. In theory, by removing the functional groups from graphene oxide, graphene layers should be obtained but unfortunately, the complete removal of the functional groups is impossible and the resultant product has several structural defects [33].

The chemical, mechanical and electrical properties of the products of the oxidation-based methods are so different from the pristine graphene that scientist prefer to use “reduced graphene oxide” term for these products. From one perspective, these methods shouldn’t be considered as a successful method for the synthesis of graphene but from another perspective, although their products aren’t suitable for some specific applications but they can provide us with some other interesting properties which weren’t available in pristine graphene (Figure 4). Up to few years ago, reduced graphene oxide and its other derivatives (e.g. graphene oxide and partially reduced graphene oxide) weren’t at the focus of the graphene researchers; mainly due to their low electrical conductivities and structural defects, but recently, in several applications such as catalysis [34], supercapacitors [35], hydrogen storage [36], microwave absorbers [37], these materials are preferred to pristine graphene.



Figure 4. Picturing two different viewpoints against reduced graphene oxide. Considering the car in (a) as pristine graphene, some researchers consider the reduced graphene oxide as the damaged car shown in (b) but the car in (c) can also represent the reduced graphene oxide because although it is not suitable for routine applications but on snow, it is preferred to the car shown in (a).

Pristine graphene is a semimetal material with a zero bandgap [38] but the introduction of the functional groups can lead to a bandgap opening [39] and as it will be discussed in greater details in the next sections, the size of this bandgap is easily tunable by controlling the functionalization degree [40]. As another example, it has been shown that presence of defects can increase the charge storage capacity of the supercapacitors 4-folds when graphene is replaced by reduced graphene oxide [35]. Hence, rather than considering the reduced graphene oxide as a defective form of graphene, it is better to classify it as a new group of carbon-based materials and benefit from the unique opportunities of this new class. This is also one of the main ideas behind the current work where semiconducting property of the graphene oxide has been used for deposition (photocatalytic deposition) of the platinum nanoparticles from a solution containing Pt^{4+} ions. It is also worth mentioning that due to the high production yields of the oxidation based methods, the processes that use reduced graphene oxide (and its other derivatives) are more likely to become commercialized [21].

1.3. Synthesis of graphene-noble metals composites

Up to the present time, numerous methods have been developed for the synthesis of metallic nanoparticles (MNPs) and graphene composites [1]. In almost all cases, especially for catalytic applications in which, MNPs surface area is the most important factor, or for applications in which, an expensive noble metal is used, uniform distribution of the nanoparticles and reduction of their size are of great importance [41–43]. Proper attachment of MNPs to graphene sheets and their efficient electrical connection are two other key features for a promising synthesis method [44]. The reduction of the metal from a solution in the presence of graphene sheets is a common approach in the majority of the current synthesis methods, and their differences lie in their reduction techniques [44–47]. However, despite this diversity, the reduction occurs either chemically by means of a reducing reagent [46,48–51] or electrochemically via an external power supply [44,52,53].

The chemical methods are usually simple and easily up-scalable, and they can be used for all forms of composites whether in powder form or as film. In these methods, through appropriate adjustment of the key reaction parameters such as

temperature, time and concentrations of reactants, the morphology and the size of the MNPs can be controlled [54]; however, this control is usually not effective enough. Furthermore, the particles can be reduced at every point of the solution (suspension) and their proper attachment to graphene sheets is yet another challenge. This challenge becomes much more noticeable when a noble metal is to be deposited due to its higher cost. In contrast, the electrochemical methods offer better control on the reduction process as the flow of electrons from an external source is easier to be controlled [54]. Moreover, the attachment and proper electrical connection of the MNPs to graphene sheets are guaranteed as electron current passes through the graphene sheets. Unfortunately, the application of these electrochemical methods is limited to the composites in film form and the distribution of the particles depends on the local conductivity of the various regions of this film [55].

Thus, the development of a new method which benefits from the advantageous of both chemical and electrochemical methods would be quite favorable. For instance, by attaching several nano-sized electron generators (NEGs) to every graphene sheet (Figure 5a) and being able to easily and instantly switch them on or off (Figure 5b, c). Functionalized forms of graphene (FG) with wide-enough bandgaps are ideal platforms for this purpose. It is well established that covalent attachment of functional groups to graphene sheets opens bandgap in specific regions of FG which can act as the aforementioned NEGs. These NEGs can then be switched on or off by pulsed illumination of UV light (Figure 5b, c). On each pulse, through variation of the illumination time, the number of the produced electrons (photoexcited electrons) can be controlled, which leads to the precisely-controlled growth of the MNPs over the FG sheets. After the deposition of MNPs, the functional groups of the FGs can be removed using various thermal or chemical methods. A wide range of particle size, from sub-nanometer clusters to nanometer-sized particles are attainable by this approach. The MNPs can only be reduced over the graphene sheets (not everywhere in the solution) and the electrical connection between the graphene and MNPs is certain. Furthermore, the distribution of the deposited particles is uniform due to the even distribution of the functional groups (has been studied and shown in this work).

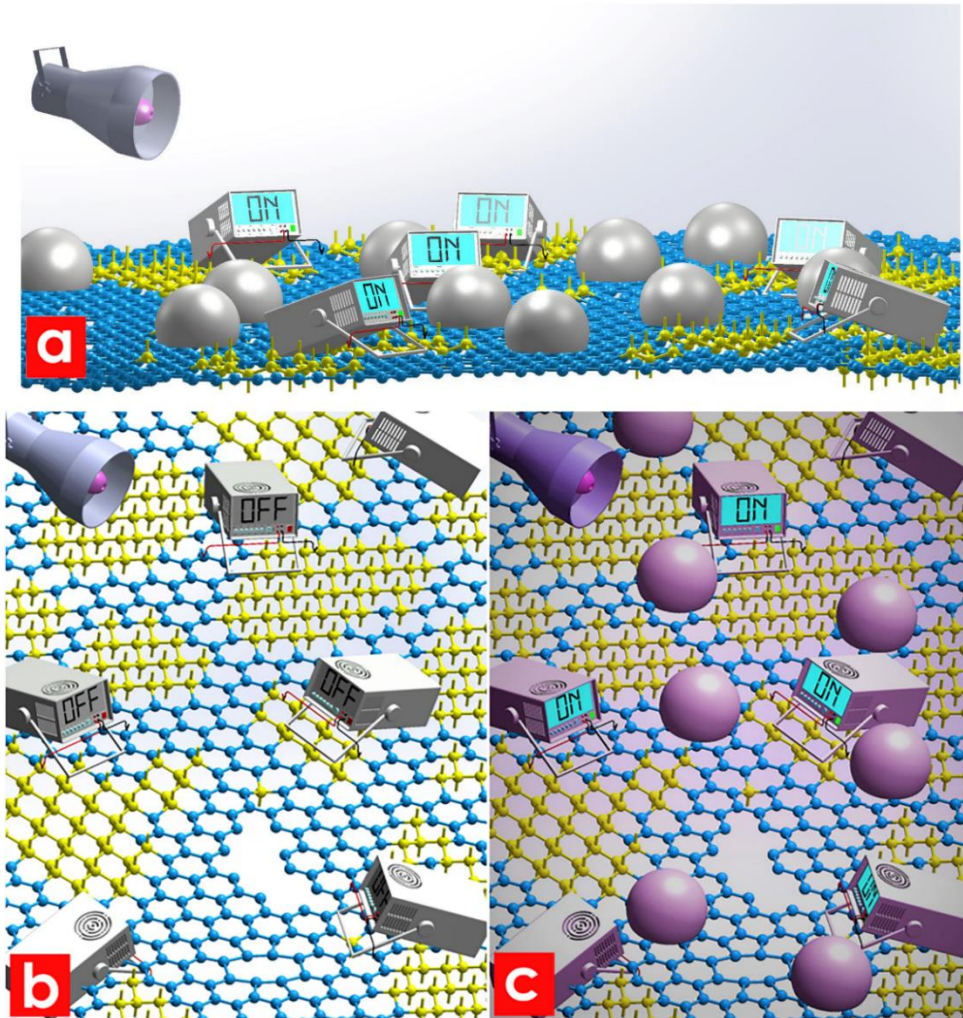


Figure 5. Schematic illustration of (a) NEG-decorated (functionalized) graphene; (b) in dark situation (NEGs are off); (c) NEG-decorated (functionalized) graphene under UV illumination where growth of Pt nanoparticles has started. The blue and yellow colored atoms have sp^2 and sp^3 hybridizations, respectively.

1.4. Partially reduced graphene oxide: Synthesis and bandgap modulation

Among numerous types of FGs, graphene oxide (GO), a heavily oxidized form of graphene, seems to be a promising candidate for the aforementioned “MNP deposition system”. While oxidization of graphite is considered as a necessary step in the graphite’s exfoliation process and for the production of reduced graphene oxide (RGO) [21], it simultaneously opens a wide bandgap in graphene[56,57]. Although numerous structural models have been proposed for GO[58,59], but its

chemical structure and the origin of its semiconductivity haven't been well-understood yet.

In general, there are two main explanations for the semiconducting behavior of GO [60]; a group of researchers attribute it to the confined electronic environment within the sp^2 hybridized domains which are surrounded by the heavily oxidized regions (with sp^3 hybridization) [57,61–64]; while other group believes that the bandgap opening, arises from the localization of the electronic environment around the attached functional groups [56,65–68]. In both theories, a direct relation between the size of the bandgap and the degree of oxidation has been established [56,57], and based on this fact, several attempts have been made to modulate the bandgap of GO, whether by controlling its oxidization process [69,70] or through a consequent partial reduction process [71–73].

While these investigations provide significant insights into the semiconducting properties of GO with various oxidation levels, but most of the studied states of GO aren't stable enough for establishing a reproducible synthesis protocol upon them. This is mainly due to the fact that during the oxidization process, depending on numerous parameters such as oxidation time and composition of the oxidization environment, various types of oxygen containing functional groups (OFGs) with different chemical stabilities attach to GO [73]. Some of these OFGs such as hydroxyl and epoxide groups can be easily detached (or decomposed) but the removal of some other groups such as carbonyl and carboxyl groups are much harder or almost impossible [57,73].

Since the chemical and the physical properties of GO, particularly its bandgap, profoundly depend on its oxidation degree (type and concentration of the attached OFGs), any alteration in amount of the OFGs will significantly affect the bandgap size and other electronic properties of the GO [57]. In fact, it has been shown that the conduction band of GO doesn't change too much with the degree of oxidation and the valence band shifts-up upon reduction and shifts-down when the concentration of OFGs increases (Figure 6) [56].

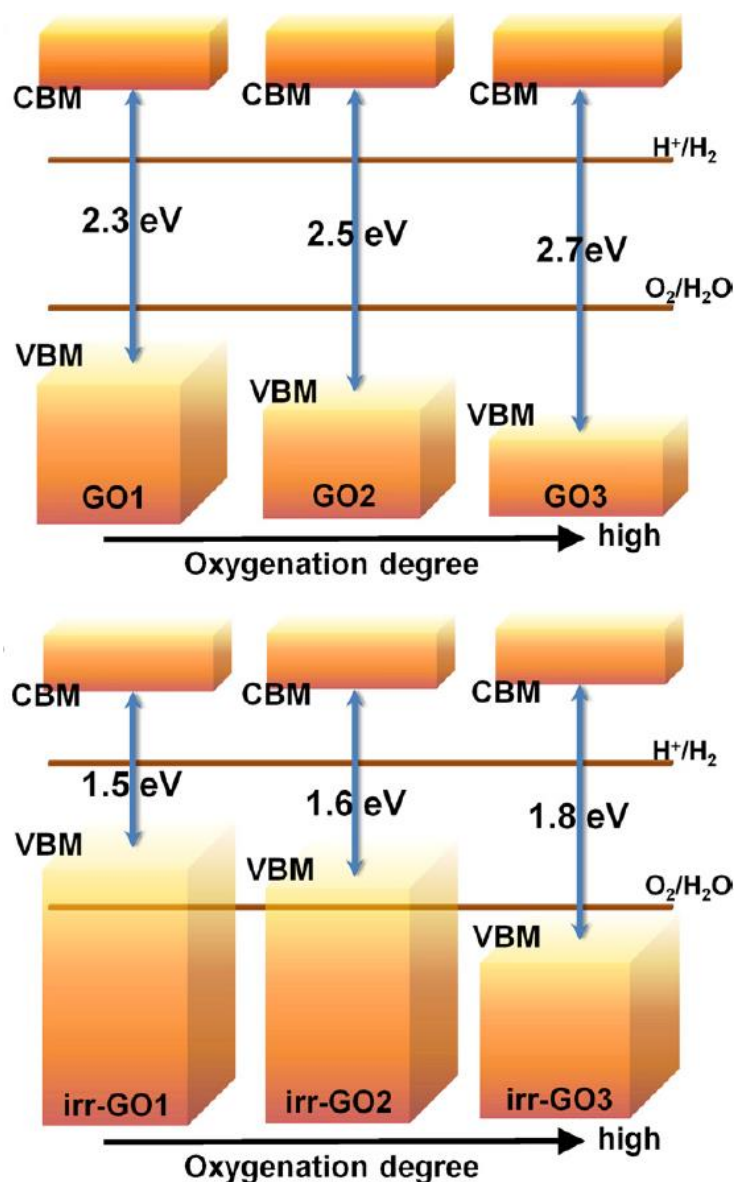


Figure 6. The dependence of the position of the valence band maximum (VBM) and conduction band minimum (CBM) of GO sheets with the variation of their oxygenation content (taken from ref. [56]).

The importance of the chemical stability of GO becomes more evident when it is exposed to mid- and high-energy radiations (e.g. UV light) or during mild thermal treatments (for synthesis purposes). It has been shown that GO can be easily reduced by heating it in pure water [74] or even illuminating it with UV light [75] without addition of any reducing agent. GO is also prone to photocorrosion in which, photoexcited electrons can reduce some of its functional groups [76]. Hence, despite its vast applications as a photocatalyst material, GO is not a suitable platform for

photocatalytic deposition of MNPs since it will experience substantial continuous changes in its chemical and physical properties during the UV illumination.

Alternatively, partially reduced graphene oxide (PRGO), in the sense that we have defined (and synthesized) in this work, due to its higher chemical stability and suitable size of its bandgap, can be used as a graphene-based photocatalyst for the deposition of MNPs. It should be noted that the partially oxidized graphene, in which, the bandgap and the chemical composition have been tuned by decreasing the duration of the oxidation process will again suffer from the same issues as GO since the partial oxidization will introduce all types of stable and unstable OFGs together but in lower concentrations. Furthermore, incomplete oxidization of graphite can lead to its inappropriate exfoliation.

For the partial reduction of graphene oxide, two approaches are conceivable; reduction by a strong reducing agent for a short period of time and reduction by a mild reducing agent. The later approach which is also used in this work is more preferred since it mainly removes the unstable and weakly bounded OFGs and the remaining product will be highly stable. The other advantage of the mild reducing agents is that the synthesis method is reproducible and the characteristics of the final products of each time synthesis are very similar since the reduction process reaches to a steady state and after that point, no considerable structural and compositional changes occur. These features have been investigated in this work in details.

Being composed of sp^2 and sp^3 hybridized carbon atoms, PRGO is dispersible in both polar and non-polar solvents (more specifically, aqueous and non-aqueous mediums) which means that it can be used for the photoelectrochemical deposition of the majority of the metals (even those with negative reduction potential versus the standard hydrogen electrode). This is also due to the fact that PRGO has a wide bandgap, whose size and band edge positions cover the required potentials for the reduction of most metal.

In addition to the versatility of the present system for deposition of various metals on RGO with precise control on the particle size, this method, thanks to the unique design of its reactor, can produce MNP-RGO composites continuously on an

industrial scale which is a crucial requirement for their commercialization. Furthermore, PRGO can form films which is desirable for the fabrication of electrodes in most of the applications.

Objectives of the Thesis

2. Objectives of the Thesis

The development of a novel method for deposition of the noble metals which have catalytic activities (mostly in fuel cell applications) was the main objective of this method. The following features were expected (and were considered) while developing this method:

- Industrially up-scalable;
- Simple yet novel;
- Precise control on the particle size (of the Pt, Pd, Ag, Au);
- Proper electrical conductivity between the particles and the graphene support.

The study of the semiconducting properties of graphene oxide, its band gap modulation and photocorrosion was the other objective of this project.

Materials and methods

3. Materials and methods

3.1. Synthetic procedures

3.1.1. Synthesis of PRGO

GO as a precursor for PRGO was synthesized according to an improved version of Hummers method but with few modifications. Typically, 1 gr of graphite (>99%, Sigma Aldrich) was added to 50 mL of sulfuric acid (H_2SO_4 , 98%, Sigma Aldrich) and the mixture was cooled down to $\sim 0^\circ\text{C}$ in an ice-water bath while being stirred. 3 gr of potassium permanganate (KMnO_4 , >99%, Merck) was added gradually to the cooled-mixture, maintaining the temperature under 5°C . The oxidation process continued for 6 hours at room temperature and finally was quenched by drop-wise addition of 250 mL of deionized water (DI). 30 mL of hydrogen peroxide (H_2O_2 , 30%, Sigma Aldrich) was added to reduce the immiscible manganese-containing species. The oxidized graphite was washed with a 1 M hydrochloric acid solution (37%, Sigma Aldrich) and DI water to near neutral pH (5.5-6).

The purified oxidized graphite was exfoliated to GO by ultrasonic treatment for 3 hours and unoxidized or unexfoliated particles were separated by a one-hour centrifugation at 8000 rpm. After determination of the solid content of the obtained supernatant, the concentration of the GO suspension was set to 0.2 gr.lit^{-1} by addition of DI water. This GO suspension was dropwise added to a same volume 4 M sodium hydroxide solution (NaOH , >98%, Sigma Aldrich). For the partial reduction of GO, the GO- NaOH mixture was stirred and refluxed for 10 h at 90°C and samples were taken after each one-hour period. The samples were denoted as PRGOX in which, X corresponds to the duration of the reduction process in hour (e.g., PRGO6 corresponds to a sample which has been refluxed at 90°C for 6 h). The PRGO samples were thoroughly washed with DI water to neutral pH.

3.1.2. Photocatalytic deposition of platinum on PRGO

For proper penetration of the UV light through the whole quartz tube, dilute suspensions of PRGO (50 mg.L^{-1}) were prepared. Hexachloroplatinic acid (H_2PtCl_6 , 8 wt. % solution in water, Sigma Aldrich) was added to the suspension as the Pt^{4+} ions source (20 wt. % with respect to PRGO), and ethanol (5 vol. % with respect to the total volume) was added as hole-scavenger[77]. Dissolved oxygen gas was

thoroughly flushed out of the suspension by injection of the N₂ gas for 30 min. Although the suspension container and circulation paths were completely sealed from oxygen penetration but to exert a positive pressure inside the reactor and to remove the produced gases during the reactions, the injection of the N₂ continued all along the photocatalytic deposition process. After specific periods of UV illumination, samples were taken and immediately washed by centrifugation. As-obtained precipitates were then dispersed in DI water by means of gentle ultrasonication in an ultrasonic bath for 1 h. Ascorbic acid (C₆H₈O₆, 99%, Sigma Aldrich) was added to the suspensions (1/1 wt. ratio with respect to the initial PRGO weight) and were heated at 90°C for 1 h. The samples were slowly cooled down to room temperature and washed with DI water to obtain the final composites. The samples were denoted as PtRGOT in which, T corresponds to the UV-illumination time in minutes (e.g., PtRG015 corresponds to a sample which has been illuminated with UV light for 15 min).

3.1.3. Photocatalytic deposition of palladium on PRGO

As the synthesis of palladium with RGO composite was carried out as a proof of the concept, only a 50 wt. % composite was synthesized and the 100% exposure tube was used. Palladium (II) chloride (PdCl₂, 60% Pd, Fluka) was first dissolved in small amount of hydrochloric acid and then were added to the same PRGO dispersion which is described in section 3.1.2. Again, the suspension (in the same reactor) was flushed out of oxygen and was illuminated by the UV light for 2 hours. After collection and washing, the final reduction was carried out in ascorbic acid (1/1 wt. ratio with respect to the initial PRGO weight) at 90°C for 1 h. The obtained product was denoted as PdRGO.

3.1.4. Photocatalytic deposition of gold on PRGO

Similar to the PdRGO sample, as the synthesis of gold-RGO composite was carried out as a proof of the concept, only a 50 wt. % composite was synthesized and the 100% exposure tube was used. Gold (III) chloride hydrate (HAuCl₄.xH₂O, 99.999% trace metals basis, Aldrich) was used with the same PRGO dispersion which is described in section 3.1.2. Exactly the same photodeposition and final

reduction processes as section 3.1.3 were utilized and the obtained product was denoted as AuRGO.

3.1.5. Photocatalytic deposition of silver on PRGO

Similar to the PdRGO and AuRGO samples, since the synthesis of silver-RGO composite was carried out as a proof of the concept, only a 50 wt. % composite was synthesized and the 100% exposure tube was used. Silver nitrate (AgNO_3 , 99.5%, Sigma Aldrich) was used with the same PRGO dispersion which is described in section 3.1.2. Exactly the same photodeposition and final reduction processes as section 3.1.3 were utilized and the obtained product was denoted as AgRGO.

3.2.Reactor design

As schematically shown in Figures 7a-c, the reactor consists of a cylinder (15 cm diameter and 55 cm length) with a polished aluminum lining. The aluminum was opted as lining because of its superior UV reflectivity. Five 55W UV-C lamps (Philips TUV PL-L 55W/4P HF 1CT/25) were installed inside the cylinder and the quartz tube was fixed along the central axis of the cylinder. A high-speed fan was installed at one end of the cylinder to air-cool the lamps and an ice-water bath was utilized for cooling down the reaction suspension. The temperature of the suspension was monitored before and after being illuminated by the UV light which never exceeded 3°C and 7°C, respectively. A magnetic pump operating at its maximum rate (16 L.min⁻¹) was used for circulation of the suspension.

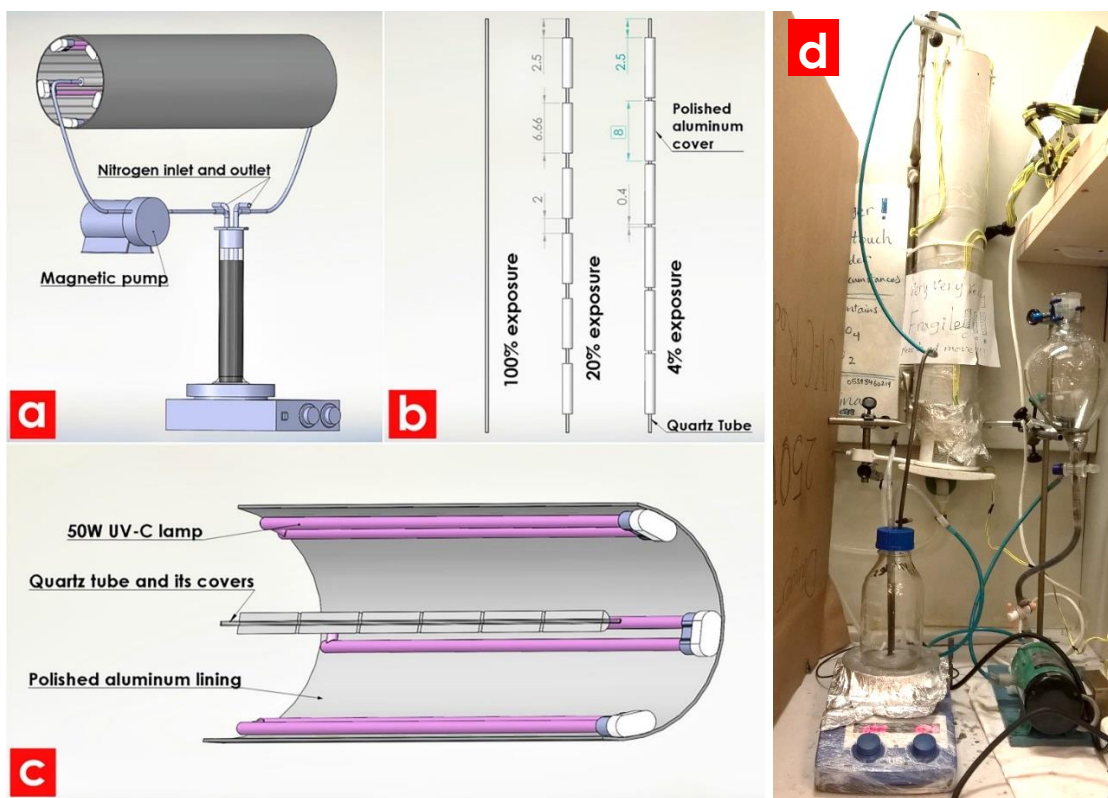


Figure 7. Schematic and real images of the photocatalytic deposition reactor; (a) the main components of the reactor; (b) quartz tubes with different exposure lengths (cm) to control the duration of UV illumination (duration of the pulses); (c) cross-sectional view of the deposition compartment demonstrating the arrangement of the UV lamps and the quartz tube; (d) real image of the reactor.

3.3. Instrumentation

A Shimadzu UV–visible spectrophotometer (UV-2550) was used to measure the UV–Vis absorption spectra. A FEI Tecnai 20 transmission electron microscope with a field emission gun was used for TEM imaging. The X-ray diffraction (XRD) patterns were recorded with a Bruker AXS advance powder diffractometer equipped with a Siemens X-ray gun, using Cu K_{α} radiation ($\lambda = 1.5406 \text{ \AA}$). Raman spectroscopy measurements were carried out using a 532 nm laser source in a Renishaw InVia Reflex Raman microscopy system. The concentration of the OFGs on GO and reduction of the RGO and Pt were studied by an X-ray photoelectron spectroscopy (XPS) instrument with a monochromatic Al K_{α} radiation source (1486.6 eV) and a hemispherical energy analyzer (Specs EA 10 Plus) operating in a vacuum better

than 10^{-7} Pa. Spectral Data Processor (SDP, V. 4.1) software was employed for curve fittings and atomic percent calculations of XPS spectra.

Results and discussions

4. Results and discussions

4.1. Partial reduction of GO and bandgap modulation

The reduction of GO by means of basic solutions (such as sodium hydroxide) has been a matter of discussion in recent years. The reactions of GO with these solutions are so bewildering that some researchers, to interpret their observations, have cast doubt on the widely accepted structural models of GO. They believe that GO is composed of a lightly oxidized graphene sheet and absorbed oxidative debris. They have claimed that the attached species are responsible for most of the electronic and optical properties of GO and the basic solutions just wash out those moieties [60,78]. But recently, Naumov et al., by comparing the optical properties of an artificially fabricated two component system (composed of a lightly functionalized graphene and oxidative moieties) with those of GO, has shown that the previously established models for GO are still valid and the OFGs are directly attached to the basal plane of graphene [60]. Although GO's two component structural model doesn't seem to be true but its reactions with basic solutions cannot completely be considered as a reduction reaction. In fact, our results as shown in Figures 9 and 10, demonstrate that even long-time treatments of GO with concentrated NaOH solutions cannot lead to the full reduction of GO and considerable amounts of OFGs will remain. Most of PRGO's characteristics such as hydrophilicity, film formation tendency and its color (dark brown) have more similarities with those of GO rather than RGO.

4.2. UV-vis spectroscopy and bandgap calculations

UV-vis absorbance spectra (Figure 8a) were used to study the changes in optical properties and size of the bandgap during the NaOH treatment of GO. The main absorbance peak at ~ 216 nm (in GO) arising from the $\pi \rightarrow \pi^*$ (C=C) transition [61] gradually redshifts to ~ 250 nm (in PRGO8 and PRGO10). A direct relation between the redshift of this peak and the degree of reduction is well established and greater shifts have been reported for RGO (>265 nm) [79,80]. A careful inspection of the Figure 2a reveals that the rate of peak shift has significantly decreased after 6 hours of NaOH treatment and in last 2 hours there hasn't been any noticeable change in the main peak's position.

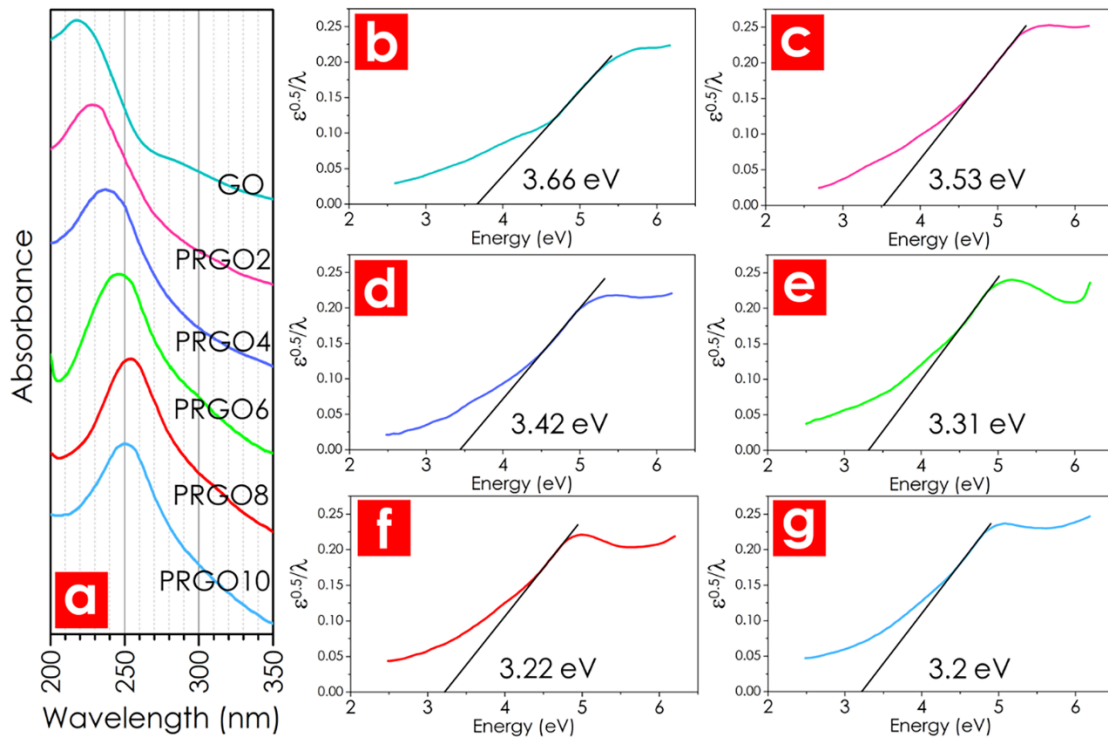


Figure 8. (a) Normalized UV-Vis spectra of GO and PRGO2-10 (an offset to the absorbance has been applied to make the peak shift more visible); Application of Tauc plot for optical band gap calculation of (b) GO; (c) PRGO2; (d) PRGO4; (e) PRGO6; (f) PRGO8; (g) PRGO10.

The optical bandgaps were calculated from the UV-vis absorbance spectra by means of Tauc's relations ($\omega^2 \epsilon = (\hbar\omega - E_g)^2$) and plotting the $\epsilon^{0.5}/\lambda$ against $1240/\lambda$; in which, ϵ is the absorbance, ω is the angular frequency and λ is the wavelength in nm [73]. The extrapolation of the linear regions of these plots to the X-axis gives the optical bandgap value [81]. As it is evident in Figures 8b-g, the band gap decreases from 3.66 eV to 3.2 eV and the bandgaps of PRGO8 and PRGO10 have similar values. These observations support the idea that the optical changes during the NaOH treatment reaches to a steady state after a specific period of time (8 hours).

4.3. Raman spectroscopy

Raman spectroscopy is a strong tool for monitoring the structural changes during the oxidation and reduction of graphene and for this purpose, the D (1342) and G (1587) bands and their relative intensities are of a great interest. Pristine

graphene's Raman spectrum has a strong G band and almost no D band [82]. The D band begins to rise by the introduction of structural defects but with a non-monotonic trend. In a low-defect regime where the perfect structure of graphene dominates, by addition of each defect, the intensity of D band increases but after a specific point, further addition of defects leads to the amorphization of the crystalline structure and attenuation of all Raman peaks [83]. Hence, in a highly defective structure like GO, the increase in the relative intensities of D and G bands (I_D/I_G) can be ascribed to the recovery of the sp^2 -hybridized domains [84]. As it is shown in Figure 9, the I_D/I_G has increased from 0.85 to about 0.97 after 4 hours of NaOH treatment but after that (in last 6 hours) there has been virtually no change in its value (0.97→0.99).

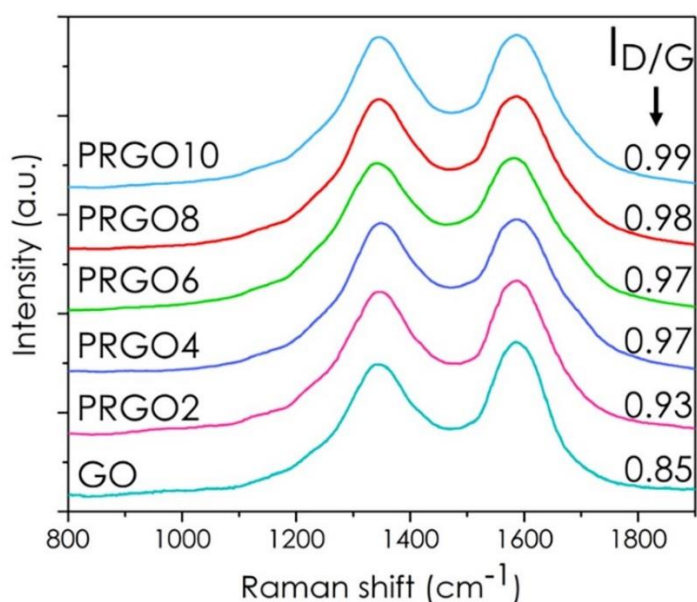


Figure 9. Normalized Raman spectra of GO and PRGO2-10 excited with a 532 nm laser source.

4.4.X-ray photoelectron spectroscopy for monitoring the reduction

The XPS analysis of GO and deconvolution of its C_{1s} peak (Figure 10) clearly reveals that the initial GO is fully oxidized and its OFGs consist of at least four major groups namely, hydroxyl, epoxide, carbonyl and carboxyl groups which are located at 285 eV, 285.7 eV, 287 eV and 287.5 eV respectively. Two other peaks at 284.5 eV

and 285 eV are also assigned to the sp^2 and sp^3 hybridizations of carbon atoms, respectively [58,59,84]. These assignments were based on theoretical predictions of core level shifts and on reported spectra containing the particular oxygen functional groups [21].

As it is evident, a small fraction of the carbon atoms has sp^2 hybridization while hydroxyl and epoxide groups have the highest concentrations. In order to monitor the concentration of the OFGs during the reduction process and for comparison purposes, all C_{1s} peaks of the PRGOs were deconvoluted with almost similar deconvolution parameters. After correction of the Shirley background and normalization of the data, The XPS peaks were fitted to Voigt functions having 80% Gaussian and 20% Lorentzian components. To minimize the chi-square of the fitting, the positions of the deconvolution components were allowed to move no more than ± 0.1 eV (in most of the cases, 0 or 0.05 eV). The maximum value of the FWHMs were limited to 1 ± 0.1 eV except for the two last components at 287 and 287.5 (mostly carboxyl) which evidently require larger FWHM values ($1.3 \sim 1.5 \pm 0.1$ eV) for proper fitting results [85].

Considering the changes in the deconvoluted components of C_{1s} peaks during the NaOH treatment (Figure 10), the hydroxyl and epoxide groups, in comparison with two other major groups (carbonyl and carboxyl groups), have experienced much larger variations. In fact, the variations of the carbonyl and carboxyl groups (17.6 \rightarrow 14.8 and 9 \rightarrow 8.6, respectively) are so small that they can be easily neglected. This observation is in good consistency with the proposed mechanisms for the reduction of GO with alkaline solutions.

It has been theoretically shown that an external electric field in the vicinity of GO (e.g. due to the high concentration of Na^+ ions), can weaken the C–O bonds in hydroxyl and epoxide groups and lower the GO's reduction barrier. Subsequently, in an aqueous solution with a high-enough concentration of alkaline species (e.g. NaOH), hydroxyl and epoxide groups can be reduced through a series of protonation, deprotonation and epoxide ring-opening reactions [86]. Based on the experimental observations, another reaction between basic solutions and GO has been proposed which comprises of the cleavage of graphene's basal plane C=C bonds and transformation of the hydroxyl groups to first, carbonyl groups and then,

CO₂ gas and carbon vacancies [87]. This mechanism may explain why in Raman spectra (after the 4th hour), in spite of the OFGs removal, the I_D/I_G doesn't change noticeably. Although numerous reports have been published on the reduction of GO by alkaline solutions but very few discussions exist on its underlying mechanism and it hasn't been fully understood yet. However, in almost all proposed mechanisms [86–88], the hydroxyl and epoxide groups are mainly involved in the reduction reactions.

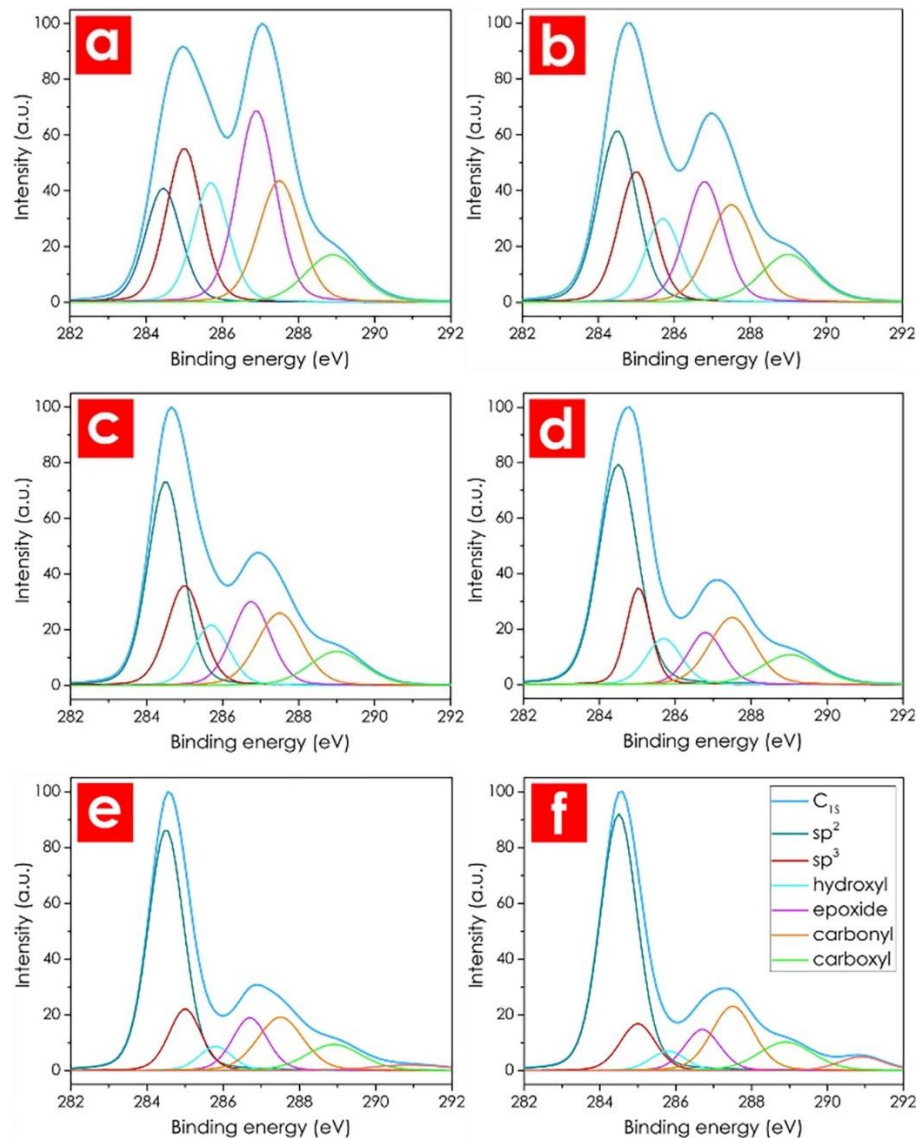


Figure 10. Deconvoluted XPS C_{1s} peak of (a) GO, (b) PRGO2, (c) PRGO4, (d) PRGO6, (e) PRGO8, and (f) PRGO10 showing gradual elimination of OFGs (assignment of the colors is similar from a-f).

Figure 11 has summarized the different trends of the chemical composition, optical bandgap and Raman spectrum's $I_{D/G}$ changes with respect to the NaOH treatment time in one graph. Considering the $I_{D/G}$ as an estimation of the sp^2 domains recovery and comparing its trend with variations of the chemical composition and the bandgap changes, it can be inferred that the semiconducting behavior of GO mainly arises from the localization of the electronic environment around the attached functional groups. Furthermore, we have shown that the NaOH treatment of GO (up to a steady state; in our experiment after 8 hours), will lead to a stable graphene-based photocatalyst material which can be used as a platform for a reproducible photocatalytic deposition system.

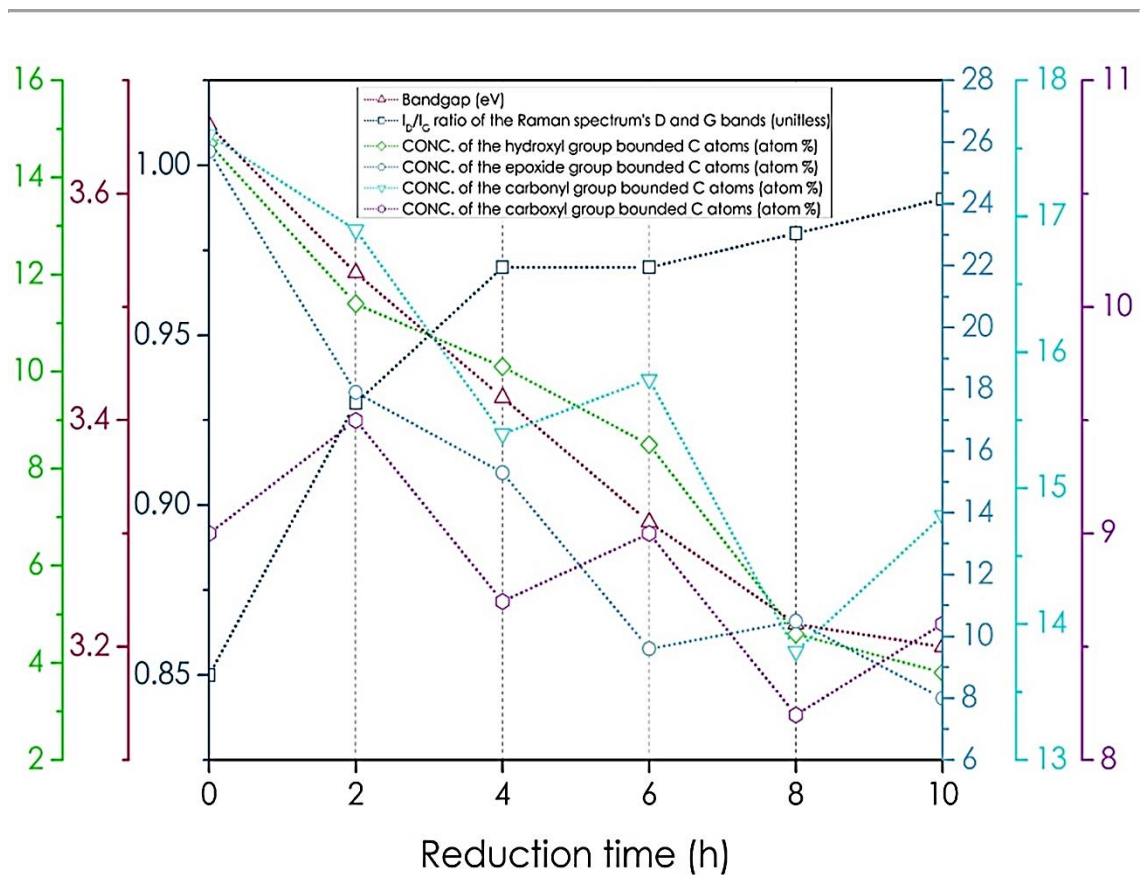


Figure 11. Evolution of optical bandgap, alteration of I_D to I_G ratio (I_D/I_G) of the Raman spectrum's D and G bands, and concentration changes of hydroxyl, epoxide, carbonyl and carboxyl groups with respect to the reduction time (treatment with NaOH) in a single graph for comparing the trends.

4.5.X-ray photoelectron spectroscopy for photostability studies

To compare the photocorrosion of PRGO and GO during long time UV-exposures, we circulated the deoxygenated suspensions of GO and PRGO8 inside our UV reactor (with 100% exposure tube) for 12 hours and the XPS results are shown in Figure 12. Evidently, PRGO8 hasn't experienced noticeable compositional changes within the first 4 (and even 8) hours of exposure which is quite enough for our photocatalytic deposition reactions while GO has continuously lost its functional groups even until the 12th hour of the UV irradiation. The mechanisms for UV-driven photocorrosion over GO sheets have been discussed in great details in previous works [56,89]. It is believed that the photo generated electron-hole pairs on GO sheets are involved in this reaction. The photogenerated electrons reduce the oxygen functional groups and leave behind a defect carbon sites.

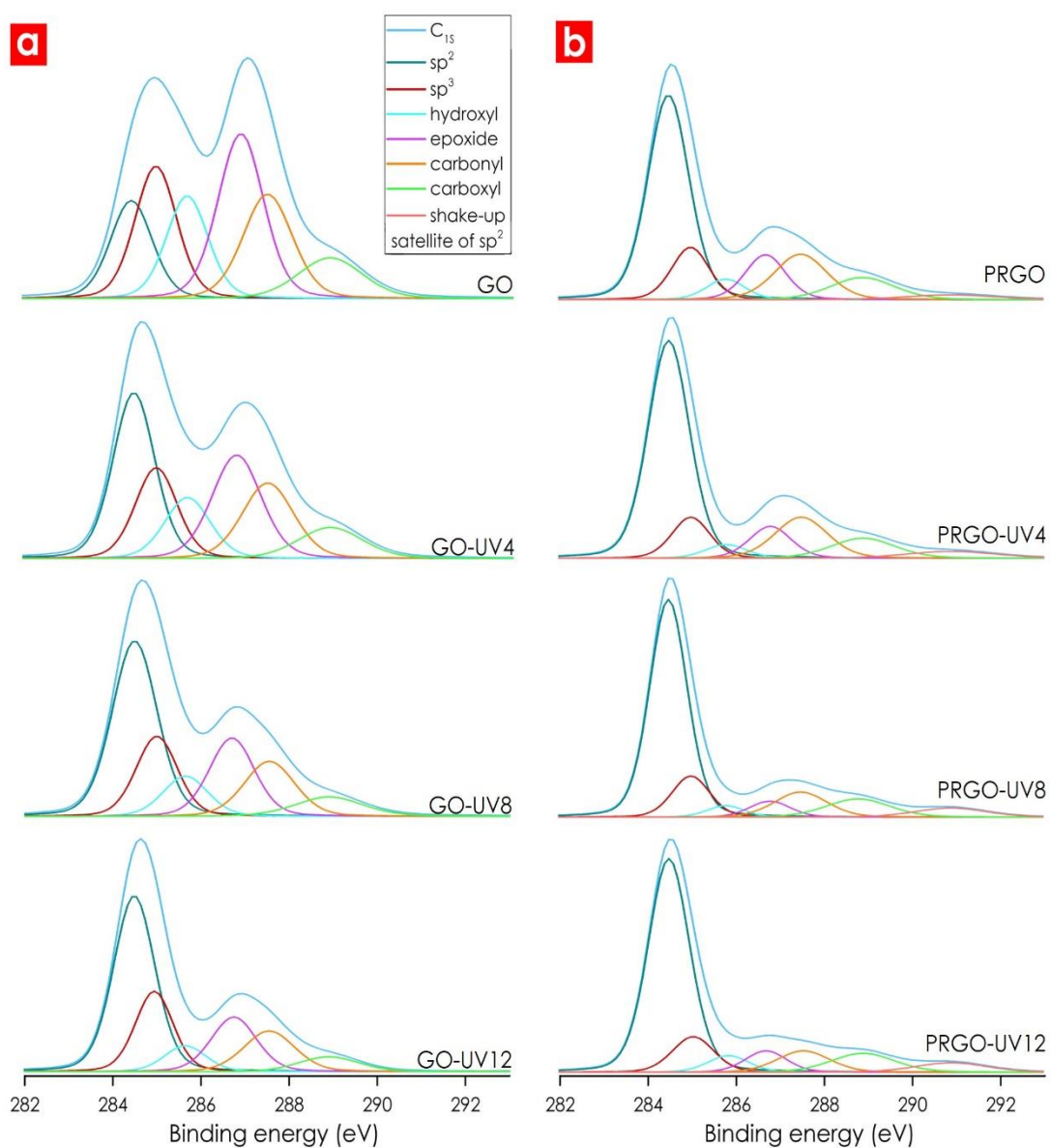


Figure 12. XPS analysis for monitoring the photostability of (a) GO and (b) PRGO8 after 4, 8 and 12 h exposure to UV light (for instance, GO-UV8 corresponds to a sample of GO which has been exposed to UV light for 8 hours).

4.6.X-ray diffraction analysis

The XRD patterns (Figure 13) suggest a hybrid nature for PRGO. Graphite's XRD pattern has a dominant peak at $2\theta=26.4^\circ$ which according to the Bragg's law, corresponds to the interlayer distance of 3.37 Å. After oxidation of graphite, due to the attachment of the OFGs, the interlayer distance significantly increases to ~ 10 Å

($2\theta=8.45^\circ$) in GO's pattern but after the NaOH treatment (in PRGO8), as a result of partial deoxygenation of GO, the interlayer spacing decreases to $\sim 7.3 \text{ \AA}$ ($2\theta=12^\circ$) and an amorphous hill evolves around $2\theta=25^\circ$ which is a characteristic feature of RGO. The crystalline structure and the deposition of the noble metals (Pt, Pd, Au, Ag) are also verified by XRD analysis (Figure 14).

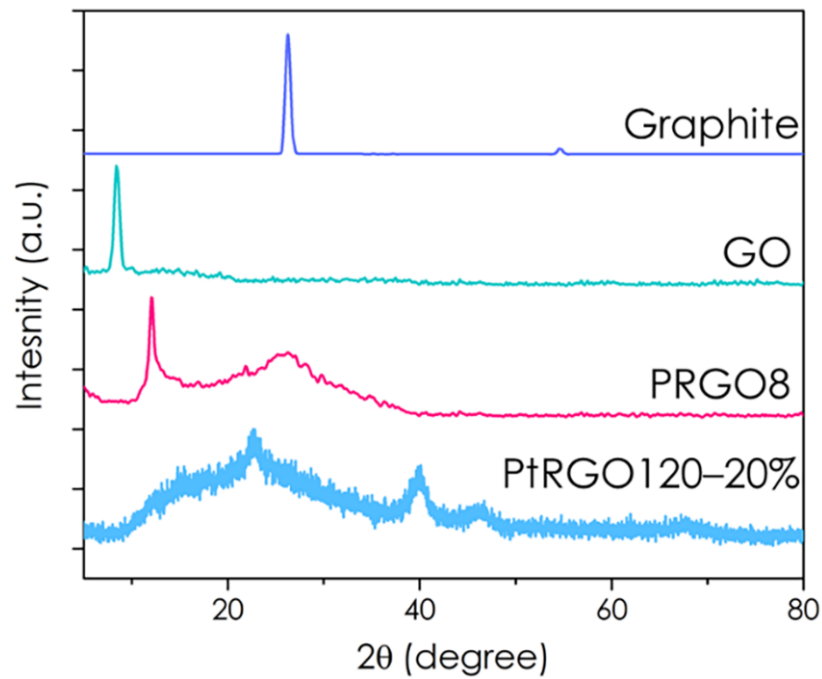


Figure 13. Normalized XRD patterns of graphite, GO, PRGO8 and PtRGO120-20%.

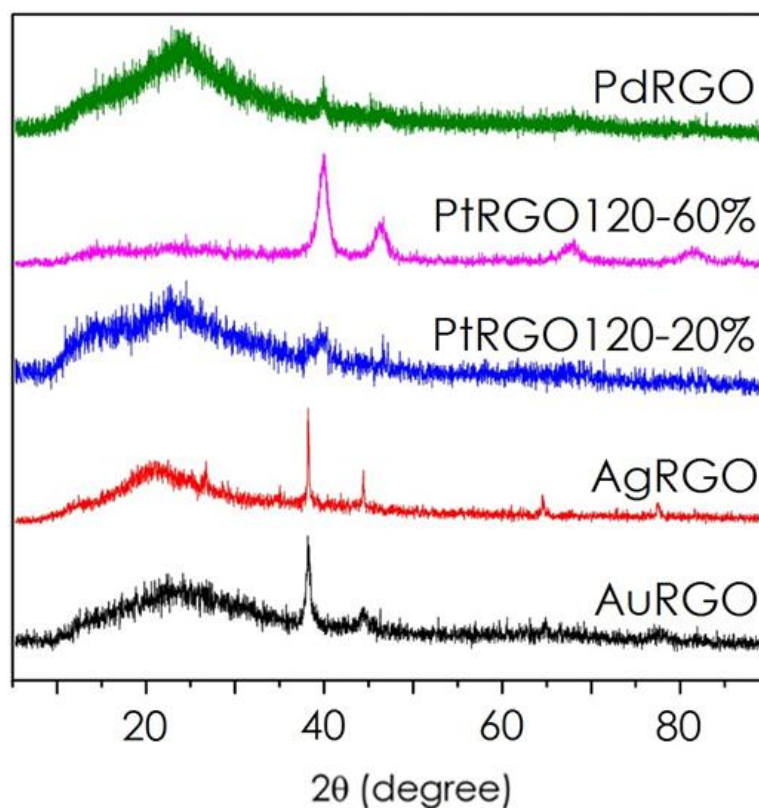


Figure 14. Normalized XRD patterns of PdRGO, PtRGO120-60%, PtRGO120-20%, AgRGO and AuRGO.

4.7. TEM studies of Pt deposition

As shown in Figure 7b, quartz tubes with three different exposure lengths (100%, 20% and 4%) were used for the photocatalytic deposition of Pt particles on PRGO8. Using the 4% exposure tube, desirable Pt loadings were achieved after very long reaction times (>10 h). The required time for 20% and 100% exposure tubes were reasonable and the distribution of the particles as shown in Figure 15a and c were uniform. The mean particle size for the 20% exposure tube and 120 mins UV illumination (Figure 15b) was about 0.9 nm, while for the 100% exposure tube, 60 mins of UV illumination resulted in larger mean particle size (~2.2 nm). As it can be seen from the inset histograms in Figs. 15b and d, the size distribution of the particles for both cases are narrow.

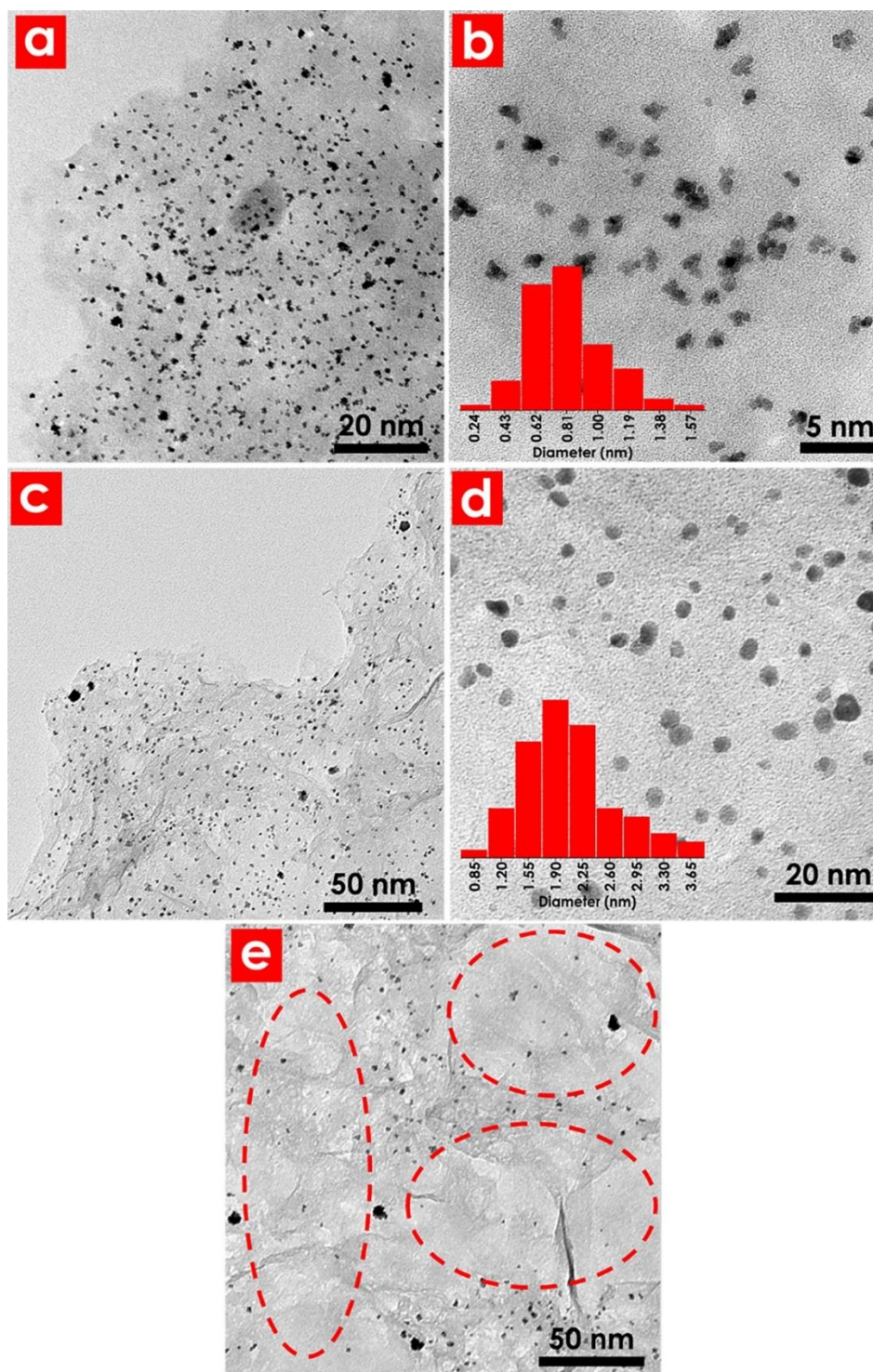


Figure 15. (a) TEM image of PtRGO120-20% showing the uniform distribution of the Pt nanoclusters; (b) TEM image and corresponding size histogram (inset) of the PtRGO120-20% showing the morphology of the Pt nanoclusters; (c) TEM image of PtRGO60-100% showing the uniform distribution of the Pt nanoparticles; (d) TEM image and corresponding size histogram (inset) of the PtRGO60-100% showing the morphology of the Pt nanoparticles; (e) TEM image of a composite which has been produced at the same conditions as PtRGO60-100% but with replacing the PRGO8 with GO.

Interestingly, the morphology of the Pt nanoparticles is different for 20% and 100% exposure tubes. In 20% exposure tube, the particles have irregular shapes which can be attributed to the shorter pulse illumination of UV light, while the product of 100% exposure tube has more regular shapes. When studying the TEM images of the GO and Pt composites (Figure 15e), in which the PRGO8 was replaced with GO in the same synthesis procedures (with 100% exposure tube and 60 min UV illumination), we noticed that there are some areas where deposition of Pt hasn't occurred while in other areas, Pt deposition is very similar to the PRGO8 samples. This observation can be attributed to the photocorrosion of GO during the UV illumination in which photoexcited electrons, in a competition with Pt^{4+} ions have been consumed by the unstable OFGs. This competitive consumption of electrons by the oxygen containing species is the main reason for the deoxygenation of the reaction suspensions at the beginning of the synthesis processes (see Materials and methods section).

4.8.X-ray photoelectron spectroscopy for photocatalytic reduction studies

The photocatalytic reduction of the noble metals were investigated by XPS analysis (Figure 16) and for this purpose, the samples were tested before performing the final ascorbic acid reduction step. The survey spectra (Figure 16a) confirms the successful deposition of the noble metals and the deconvolution of the Pt_{4f} peak shows no sign of non-metallic form of Pt which refers to its complete photocatalytic-reduction [90]. Figure 16a also contains strong oxygen peaks since the composites haven't been treated with ascorbic acid yet but after the final reduction step, as shown in Figure 16c, majority of the remaining OFGs have been removed and further removal of the OFGs is virtually impossible.

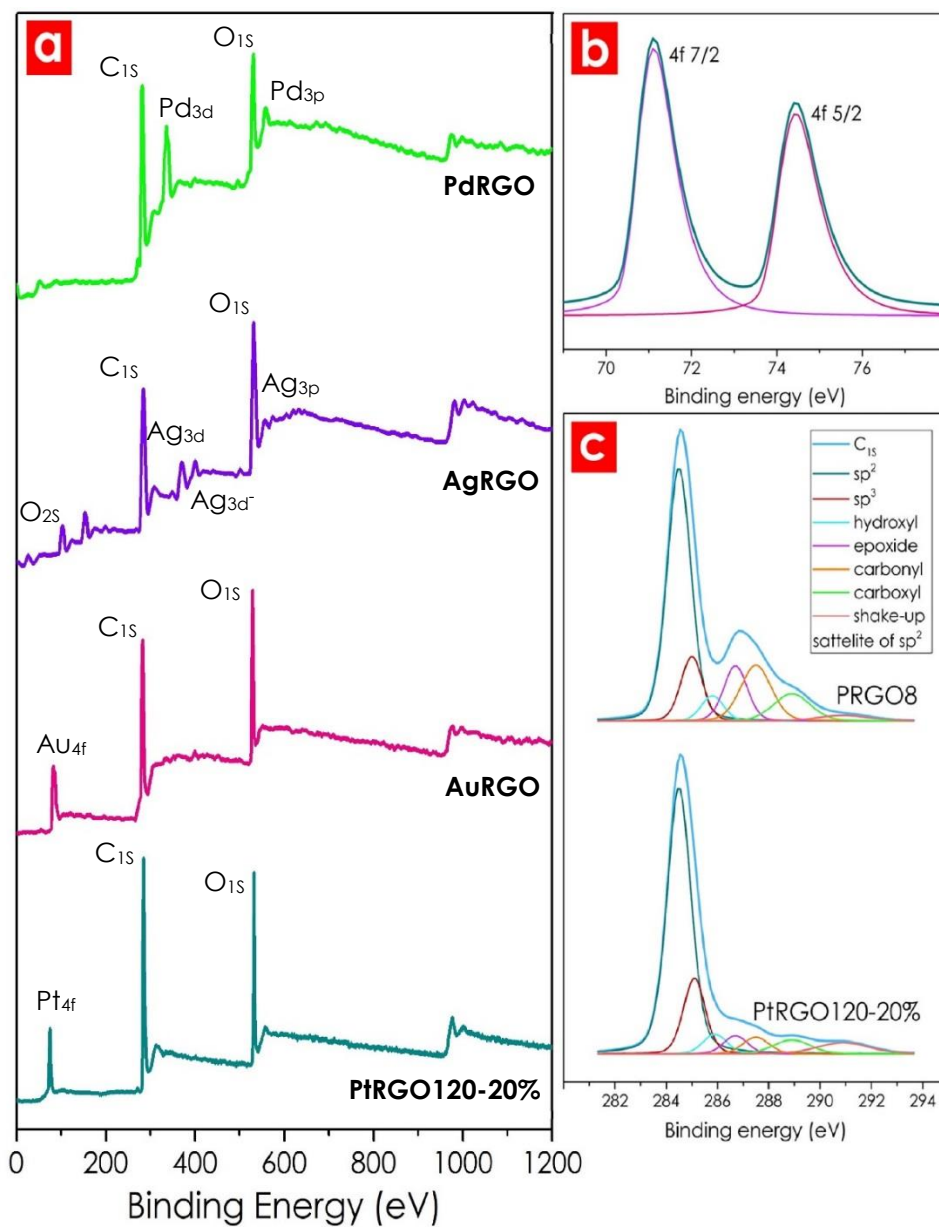


Figure 16. (a) XPS survey spectrum before treatment with ascorbic acid; (b) XPS Pt_{4f} peak of the PtPRGO120-20% sample; (c) XPS C_{1s} peak of PRGO8 and PtRGO120-20% which shows the removal of the majority of the OFGs.

Conclusions

6. Conclusions

In this work, we have shown that the semiconducting properties of GO can be utilized for the synthesis of MNP-RGO composites but for developing a reproducible synthesis method a pretreatment and modulation of the GO's properties is necessary. It has been shown that the treatment of GO with highly-concentrated NaOH solutions can only lead to the partial reduction of GO and some of its stable functional groups such as carbonyl and carboxyl groups will remain almost intact.

By simultaneously comparing the variations of the chemical composition, crystalline structure and optical bandgap during the NaOH treatment of GOs, we have found evidences that support the idea that the localization of the electronic environment around the attached functional groups is responsible for the semiconducting behavior of the GO. We have shown that PRGO can act as a stable photocatalytic MNP deposition platform and the growth of the particles can be controlled precisely with the pulsed illumination of UV light in this system. Although the deposition of 4 metals (Pt, Pd, Au and Ag) have been studied in this work, but our developed method can be easily used for industrial-scale synthesis of other MNP-RGO composites as well.

References

References

- [1] C. Tan, X. Huang, H. Zhang, Synthesis and applications of graphene-based noble metal nanostructures, *Mater. Today*. 16 (2013) 29–36. doi:10.1016/j.mattod.2013.01.021.
- [2] A. Yürüm, S.A. Gürsel, B.S. Okan, A. Taralp, F. Bakan, I. Letofsky-Papst, Y. Yürüm, Size and Dispersion Control of Pt Nanoparticles Grown Upon Graphite-Derived Nanosheets, *Chem. Eng. Commun.* 202 (2015) 1645–1656. doi:10.1080/00986445.2014.968714.
- [3] D.B. Gorle, V. Velacheri Kumman, M.A. Kulandainathan, Highly efficient, large surface area and spherically shaped Pt particles deposited electrolytically synthesized graphene for methanol oxidation with impedance spectroscopy, *Int. J. Hydrogen Energy*. 42 (2017) 16258–16268. doi:10.1016/j.ijhydene.2017.05.160.
- [4] H.-Y. Chuang, H.-H. Tseng, T.-Y. Chung, M.-S. Yu, Synthesis and characterization of activated carbon-platinum composites and effect on hydrogen storage rate, *Asia-Pacific J. Chem. Eng.* 7 (2012) S118–S124. doi:10.1002/apj.659.
- [5] L. Işikel Şanlı, V. Bayram, S. Ghobadi, N. Düzen, S. Alkan Gürsel, Engineered catalyst layer design with graphene-carbon black hybrid supports for enhanced platinum utilization in PEM fuel cell, *Int. J. Hydrogen Energy*. 42 (2017) 1085–1092. doi:10.1016/j.ijhydene.2016.08.210.
- [6] M.M. Shaijumon, S. Ramaprabhu, N. Rajalakshmi, Platinum/multiwalled carbon nanotubes-platinum/carbon composites as electrocatalysts for oxygen reduction reaction in proton exchange membrane fuel cell, *Appl. Phys. Lett.* 88 (2006) 253105. doi:10.1063/1.2214139.
- [7] P. Pieta, E. Grodzka, K. Winkler, M. Warczak, A. Sadkowski, G.Z. Zukowska, G.M. Venukadasula, F. D'Souza, W. Kutner, Conductive, Capacitive, and Viscoelastic Properties of a New Composite of the C₆₀–Pd Conducting Polymer and Single-Wall Carbon Nanotubes, *J. Phys. Chem. B*. 113 (2009) 6682–6691. doi:10.1021/jp810173c.

- [8] E. Daş, S. Alkan Gürsel, L. Işikel Şanlı, A. Bayrakçeken Yurtcan, Thermodynamically controlled Pt deposition over graphene nanoplatelets: Effect of Pt loading on PEM fuel cell performance, *Int. J. Hydrogen Energy*. (2017). doi:10.1016/j.ijhydene.2017.06.108.
- [9] R.H. Baughman, A.A. Zakhidov, W.A. de Heer, Carbon Nanotubes--the Route Toward Applications, *Science* (80-.). 297 (2002). <http://science.sciencemag.org/content/297/5582/787> (accessed July 25, 2017).
- [10] R.M. Jacobberger, R. Machhi, J. Wroblewski, B. Taylor, A.L. Gillian-Daniel, M.S. Arnold, Simple Graphene Synthesis via Chemical Vapor Deposition, *J. Chem. Educ.* 92 (2015) 1903–1907. doi:10.1021/acs.jchemed.5b00126.
- [11] S. Pei, H.-M. Cheng, The reduction of graphene oxide, *Carbon N. Y.* 50 (2012) 3210–3228. doi:10.1016/j.carbon.2011.11.010.
- [12] J. Yuan, L.-P. Ma, S. Pei, J. Du, Y. Su, W. Ren, H.-M. Cheng, Tuning the Electrical and Optical Properties of Graphene by Ozone Treatment for Patterning Monolithic Transparent Electrodes, *ACS Nano*. 7 (2013) 4233–4241. doi:10.1021/nn400682u.
- [13] A. Celis, M.N. Nair, A. Taleb-Ibrahimi, E.H. Conrad, C. Berger, W.A. de Heer, A. Tejeda, Graphene nanoribbons: fabrication, properties and devices, *J. Phys. D. Appl. Phys.* 49 (2016) 143001. doi:10.1088/0022-3727/49/14/143001.
- [14] A. Orlof, J. Ruseckas, I. V. Zozoulenko, Effect of zigzag and armchair edges on the electronic transport in single-layer and bilayer graphene nanoribbons with defects, *Phys. Rev. B*. 88 (2013) 125409. doi:10.1103/PhysRevB.88.125409.
- [15] R. Eqra, K. Janghorban, H.D. Manesh, Effect of number of graphene layers on mechanical and dielectric properties of graphene–epoxy nanocomposites, *Plast. Rubber Compos.* 44 (2015) 405–412. doi:10.1179/1743289815Y.0000000037.
- [16] C. Hong, A. Wong, Z. Ek Sofer, M. Kubešová, J. Kučera, S. Mat Ejková, M. Pumera, Synthetic routes contaminate graphene materials with a whole

- spectrum of unanticipated metallic elements, (n.d.).
doi:10.1073/pnas.1413389111.
- [17] L. Vicarelli, S.J. Heerema, C. Dekker, H.W. Zandbergen, Controlling Defects in Graphene for Optimizing the Electrical Properties of Graphene Nanodevices, *ACS Nano*. 9 (2015) 3428–3435. doi:10.1021/acsnano.5b01762.
- [18] V. Georgakilas, J.A. Perman, J. Tucek, R. Zboril, Broad Family of Carbon Nanoallotropes: Classification, Chemistry, and Applications of Fullerenes, Carbon Dots, Nanotubes, Graphene, Nanodiamonds, and Combined Superstructures, (n.d.). doi:10.1021/cr500304f.
- [19] L.E.F. Foà Torres, S. Roche, J.-C. Charlier, Introduction to graphene-based nanomaterials : from electronic structure to quantum transport, n.d.
<http://www.cambridge.org/ch/academic/subjects/physics/condensed-matter-physics-nanoscience-and-mesoscopic-physics/introduction-graphene-based-nanomaterials-electronic-structure-quantum-transport?format=HB&isbn=9781107030831#iGIRMDDFSiPGuC0f.97>
(accessed July 25, 2017).
- [20] A. Ciesielski, P. Samorì, Supramolecular Approaches to Graphene: From Self-Assembly to Molecule-Assisted Liquid-Phase Exfoliation, *Adv. Mater.* 28 (2016) 6030–6051. doi:10.1002/adma.201505371.
- [21] S. Abdolhosseinzadeh, H. Asgharzadeh, H. Seop Kim, J. Hamilton, D. Blankschtein, Fast and fully-scalable synthesis of reduced graphene oxide., *Sci. Rep.* 5 (2015) 10160. doi:10.1038/srep10160.
- [22] K.S. Novoselov, Nobel Lecture: Graphene: Materials in the Flatland, *Rev. Mod. Phys.* 83 (2011) 837–849. doi:10.1103/RevModPhys.83.837.
- [23] J. Chen, M. Duan, G. Chen, Continuous mechanical exfoliation of graphene sheets via three-roll mill, *J. Mater. Chem.* 22 (2012) 19625.
doi:10.1039/c2jm33740a.
- [24] M. Yi, Z. Shen, A review on mechanical exfoliation for the scalable production of graphene, *J. Mater. Chem. A*. 3 (2015) 11700–11715.
doi:10.1039/C5TA00252D.

- [25] K.R. Paton, Scalable production of large quantities of defect-free few-layer graphene by shear exfoliation in liquids, (2014). doi:10.1038/NMAT3944.
- [26] D.W. Johnson, B.P. Dobson, K.S. Coleman, A manufacturing perspective on graphene dispersions, *Curr. Opin. Colloid Interface Sci.* 20 (2015) 367–382. doi:10.1016/j.cocis.2015.11.004.
- [27] S. Haar, M. Bruna, J. Xiang Lian, F. Tomarchio, Y. Olivier, R. Mazzaro, Δ. Vittorio Morandi, J. Moran, A.C. Ferrari, D. Beljonne, A. Ciesielski, P. Samorì, Liquid-Phase Exfoliation of Graphite into Single- and Few-Layer Graphene with α -Functionalized Alkanes, (n.d.). doi:10.1021/acs.jpcclett.6b01260.
- [28] S. Ye, J. Feng, The effect of sonication treatment of graphene oxide on the mechanical properties of the assembled films, *RSC Adv.* 6 (2016) 39681–39687. doi:10.1039/C6RA03996K.
- [29] M. V. Bracamonte, G.I. Lacconi, S.E. Urreta, L.E.F. Foa Torres, On the Nature of Defects in Liquid-Phase Exfoliated Graphene, *J. Phys. Chem. C.* 118 (2014) 15455–15459. doi:10.1021/jp501930a.
- [30] R. Narayan, S.O. Kim, Surfactant mediated liquid phase exfoliation of graphene., *Nano Converg.* 2 (2015) 20. doi:10.1186/s40580-015-0050-x.
- [31] M. Cai, D. Thorpe, D.H. Adamson, H.C. Schniepp, Methods of graphite exfoliation, (n.d.). doi:10.1039/c2jm34517j.
- [32] Y.T. Liang, M.C. Hersam, Highly Concentrated Graphene Solutions via Polymer Enhanced Solvent Exfoliation and Iterative Solvent Exchange, *J. Am. Chem. Soc.* 132 (2010) 17661–17663. doi:10.1021/ja107661g.
- [33] M.-C. Hsiao, S.-H. Liao, M.-Y. Yen, P.-I. Liu, N.-W. Pu, C.-A. Wang, C.-C.M. Ma, Preparation of Covalently Functionalized Graphene Using Residual Oxygen-Containing Functional Groups, (n.d.). doi:10.1021/am100597d.
- [34] Y. Jia, L. Zhang, A. Du, G. Gao, J. Chen, X. Yan, C.L. Brown, X. Yao, Defect Graphene as a Trifunctional Catalyst for Electrochemical Reactions, *Adv. Mater.* 28 (2016) 9532–9538. doi:10.1002/adma.201602912.
- [35] M.A. Pope, I.A. Aksay, Four-Fold Increase in the Intrinsic Capacitance of

- Graphene through Functionalization and Lattice Disorder, *J. Phys. Chem. C.* 119 (2015) 20369–20378. doi:10.1021/acs.jpcc.5b07521.
- [36] L. Wang, K. Lee, Y.-Y. Sun, M. Lucking, Z. Chen, J.J. Zhao, S.B. Zhang, Graphene Oxide as an Ideal Substrate for Hydrogen Storage, *ACS Nano.* 3 (2009) 2995–3000. doi:10.1021/nn900667s.
- [37] C. Wang, X. Han, P. Xu, X. Zhang, Y. Du, S. Hu, J. Wang, X. Wang, The electromagnetic property of chemically reduced graphene oxide and its application as microwave absorbing material, *Appl. Phys. Lett.* 98 (2011) 72906. doi:10.1063/1.3555436.
- [38] P. Rani, V.K. Jindal, Designing band gap of graphene by B and N dopant atoms, *RSC Adv.* 3 (2013) 802–812. doi:10.1039/C2RA22664B.
- [39] P.F. Bazylewski, V.L. Nguyen, R.P.C. Bauer, A.H. Hunt, E.J.G. Mcdermott, B.D. Leedahl, A.I. Kukhareenko, S.O. Cholakh, E.Z. Kurmaev, P. Blaha, A. Moewes, Y.H. Lee, G.S. Chang, Selective Area Band Engineering of Graphene using Cobalt- Mediated Oxidation, *Nat. Publ. Gr.* (2015). doi:10.1038/srep15380.
- [40] M. Acik, Y.J. Chabal, A Review on Reducing Graphene Oxide for Band Gap Engineering, *J. Mater. Sci. Res.* 2 (2012) 101. doi:10.5539/jmsr.v2n1p101.
- [41] G. Chang, H. Shu, Q. Huang, M. Oyama, K. Ji, X. Liu, Y. He, Synthesis of highly dispersed Pt nanoclusters anchored graphene composites and their application for non-enzymatic glucose sensing, *Electrochim. Acta.* 157 (2015) 149–157. doi:10.1016/j.electacta.2015.01.085.
- [42] E. Yoo, T. Okata, T. Akita, M. Kohyama, J. Nakamura, I. Honma, Enhanced Electrocatalytic Activity of Pt Subnanoclusters on Graphene Nanosheet Surface, (n.d.). doi:10.1021/nl900397t.
- [43] N. Shang, P. Papakonstantinou, P. Wang, S.R.P. Silva, Platinum Integrated Graphene for Methanol Fuel Cells, *J. Phys. Chem. C.* 114 (2010) 15837–15841. doi:10.1021/jp105470s.
- [44] T. Maiyalagan, X. Dong, P. Chen, X. Wang, Electrodeposited Pt on three-dimensional interconnected graphene as a free-standing electrode for fuel

cell application, (n.d.). doi:10.1039/c2jm16541d.

- [45] C. Liu, K. Wang, S. Luo, Y. Tang, L. Chen, Direct Electrodeposition of Graphene Enabling the One-Step Synthesis of Graphene-Metal Nanocomposite Films, *Small*. 7 (2011) 1203–1206. doi:10.1002/sml.201002340.
- [46] S. Guo, D. Wen, Y. Zhai, S. Dong, E. Wang, Platinum Nanoparticle Ensemble-on-Graphene Hybrid Nanosheet: One-Pot, Rapid Synthesis, and Used as New Electrode Material for Electrochemical Sensing, *ACS Nano*. 4 (2010) 3959–3968. doi:10.1021/nn100852h.
- [47] Y. Li, L. Tang, J. Li, Preparation and electrochemical performance for methanol oxidation of pt/graphene nanocomposites, 2009. doi:10.1016/j.elecom.2009.02.009.
- [48] Z. Luo, L. Yuwen, B. Bao, J. Tian, X. Zhu, L. Weng, L. Wang, One-pot, low-temperature synthesis of branched platinum nanowires/reduced graphene oxide (BPtNW/RGO) hybrids for fuel cells, *J. Mater. Chem.* 22 (2012) 7791. doi:10.1039/c2jm30376k.
- [49] H.-W. Ha, I.Y. Kim, S.-J. Hwang, R.S. Ruoff, One-Pot Synthesis of Platinum Nanoparticles Embedded on Reduced Graphene Oxide for Oxygen Reduction in Methanol Fuel Cells, *Electrochem. Solid-State Lett.* 14 (2011) B70. doi:10.1149/1.3584092.
- [50] E. Daş, S. Alkan Gürsel, L. Işikel Şanlı, A. Bayrakçeken Yurtcan, Comparison of two different catalyst preparation methods for graphene nanoplatelets supported platinum catalysts, *Int. J. Hydrogen Energy*. 41 (2016) 9755–9761. doi:10.1016/j.ijhydene.2016.01.111.
- [51] B. Seger, P. V. Kamat, Electrocatalytically Active Graphene-Platinum Nanocomposites. Role of 2-D Carbon Support in PEM Fuel Cells, *J. Phys. Chem. C*. 113 (2009) 7990–7995. doi:10.1021/jp900360k.
- [52] K. Kakaei, One-pot electrochemical synthesis of graphene by the exfoliation of graphite powder in sodium dodecyl sulfate and its decoration with platinum nanoparticles for methanol oxidation, *Carbon N. Y.* 51 (2013) 195–201. doi:10.1016/j.carbon.2012.08.028.

- [53] H. Wu, J. Wang, X. Kang, C. Wang, D. Wang, J. Liu, I.A. Aksay, Y. Lin, Glucose biosensor based on immobilization of glucose oxidase in platinum nanoparticles/graphene/chitosan nanocomposite film, 2009. doi:10.1016/j.talanta.2009.06.054.
- [54] C.R.K. Rao, D.C. Trivedi, Chemical and electrochemical depositions of platinum group metals and their applications, *Coord. Chem. Rev.* 249 (2005) 613–631. doi:10.1016/j.ccr.2004.08.015.
- [55] V. V Kondratiev, V. V Malev, S.N. Eliseeva, Composite electrode materials based on conducting polymers loaded with metal nanostructures, *Russ. Chem. Rev.* 85 (2016) 14–37. doi:10.1070/RCR4509.
- [56] T.-F. Yeh, J. Cihlář, C.-Y. Chang, C. Cheng, H. Teng, Roles of graphene oxide in photocatalytic water splitting, *Mater. Today.* 16 (2013) 78–84. doi:10.1016/j.mattod.2013.03.006.
- [57] K.P. Loh, Q.L. Bao, G. Eda, M. Chhowalla, Graphene oxide as a chemically tunable platform for optical applications, *Nat. Chem.* (2010). doi:10.1038/Nchem.907.
- [58] W. Gao, L.B. Alemany, L. Ci, P.M. Ajayan, New insights into the structure and reduction of graphite oxide, *Nat. Chem.* 1 (2009) 403–408. doi:10.1038/nchem.281.
- [59] Anton Lerf, Heyong He, Michael Forster, Jacek Klinowski, Structure of Graphite Oxide Revisited, (1998). doi:10.1021/JP9731821.
- [60] A. Naumov, F. Grote, M. Overgaard, A. Roth, C.E. Halbig, K. Nørgaard, D.M. Guldi, S. Eigler, Graphene Oxide: A One- versus Two-Component Material, *J. Am. Chem. Soc.* 138 (2016) 11445–11448. doi:10.1021/jacs.6b05928.
- [61] G. Eda, Y.-Y. Lin, C. Mattevi, H. Yamaguchi, H.-A. Chen, I.-S. Chen, C.-W. Chen, M. Chhowalla, Blue Photoluminescence from Chemically Derived Graphene Oxide, *Adv. Mater.* 22 (2010) 505–509. doi:10.1002/adma.200901996.
- [62] H.-C. Hsu, I. Shown, H.-Y. Wei, Y.-C. Chang, H.-Y. Du, Y.-G. Lin, C.-A. Tseng, C.-H. Wang, L.-C. Chen, Y.-C. Lin, K.-H. Chen, Graphene oxide as a promising

- photocatalyst for CO₂ to methanol conversion., *Nanoscale*. 5 (2013) 262–8. doi:10.1039/c2nr31718d.
- [63] D. Kozawa, X. Zhu, Y. Miyauchi, S. Mouri, M. Ichida, H. Su, K. Matsuda, Excitonic Photoluminescence from Nanodisc States in Graphene Oxides, *J. Phys. Chem. Lett.* 5 (2014) 1754–1759. doi:10.1021/jz500516u.
- [64] G. Xin, Y. Meng, Y. Ma, D. Ho, N. Kim, S.M. Cho, H. Chae, Tunable photoluminescence of graphene oxide from near-ultraviolet to blue, 2012. doi:10.1016/j.matlet.2012.01.047.
- [65] C. Galande, A.D. Mohite, A. V. Naumov, W. Gao, L. Ci, A. Ajayan, H. Gao, A. Srivastava, R.B. Weisman, P.M. Ajayan, Quasi-Molecular Fluorescence from Graphene Oxide, *Sci. Rep.* 1 (2011) 85. doi:10.1038/srep00085.
- [66] J. Shang, L. Ma, J. Li, W. Ai, T. Yu, G.G. Gurzadyan, The Origin of Fluorescence from Graphene Oxide, *Sci. Rep.* 2 (2012) 73005. doi:10.1038/srep00792.
- [67] X. Jiang, J. Nisar, B. Pathak, J. Zhao, R. Ahuja, Graphene oxide as a chemically tunable 2-D material for visible-light photocatalyst applications, *J. Catal.* 299 (2013) 204–209. doi:10.1016/j.jcat.2012.12.022.
- [68] R.J.W.E. Lahaye, H.K. Jeong, C.Y. Park, Y.H. Lee, Density functional theory study of graphite oxide for different oxidation levels, *Phys. Rev. B.* 79 (2009) 125435. doi:10.1103/PhysRevB.79.125435.
- [69] Z. Luo, P.M. Vora, E.J. Mele, A.T.C. Johnson, J.M. Kikkawa, Photoluminescence and band gap modulation in graphene oxide, *Appl. Phys. Lett.* 94 (2009) 111909. doi:10.1063/1.3098358.
- [70] N. Morimoto, T. Kubo, Y. Nishina, Tailoring the Oxygen Content of Graphite and Reduced Graphene Oxide for Specific Applications, *Nat. Publ. Gr.* (2016) 4–11. doi:10.1038/srep21715.
- [71] M. Lundie, Ž. Šljivančanin, S. Tomić, Electronic and optical properties of reduced graphene oxide, *J. Mater. Chem. C.* 3 (2015) 7632–7641. doi:10.1039/C5TC00437C.
- [72] M.A. Velasco-Soto, S.A. Pérez-García, J. Alvarez-Quintana, Y. Cao, L. Nyborg, L.

- Licea-Jiménez, Selective band gap manipulation of graphene oxide by its reduction with mild reagents, *Carbon N. Y.* 93 (2015) 967–973.
doi:10.1016/j.carbon.2015.06.013.
- [73] A. Mathkar, D. Tozier, P. Cox, P. Ong, C. Galande, K. Balakrishnan, A. Leela Mohana Reddy, P.M. Ajayan, Controlled, Stepwise Reduction and Band Gap Manipulation of Graphene Oxide, *J. Phys. Chem. Lett.* 3 (2012) 986–991.
doi:10.1021/jz300096t.
- [74] V. Loryuenyong, K. Totepvimarn, P. Eimburanapravat, W. Boonchompoo, A. Buasri, Preparation and Characterization of Reduced Graphene Oxide Sheets via Water-Based Exfoliation and Reduction Methods, *Adv. Mater. Sci. Eng.* 2013 (2013) 1–5. doi:10.1155/2013/923403.
- [75] Y.H. Ding, P. Zhang, Q. Zhuo, H.M. Ren, Z.M. Yang, Y. Jiang, A green approach to the synthesis of reduced graphene oxide nanosheets under UV irradiation, *Nanotechnology.* 22 (2011) 215601. doi:10.1088/0957-4484/22/21/215601.
- [76] W.-C. Hou, Y.-S. Wang, Photocatalytic Generation of H₂O₂ by Graphene Oxide in Organic Electron Donor-Free Condition under Sunlight, *ACS Sustain. Chem. Eng.* 5 (2017) 2994–3001.
doi:10.1021/acssuschemeng.6b02635.
- [77] G. Williams, B. Seger, P. V Kamat, TiO₂-Graphene Nanocomposites. UV-Assisted Photocatalytic Reduction of Graphene Oxide, (n.d.).
doi:10.1021/nn800251f.
- [78] J.P. Rourke, P.A. Pandey, J.J. Moore, M. Bates, I.A. Kinloch, R.J. Young, N.R. Wilson, The Real Graphene Oxide Revealed: Stripping the Oxidative Debris from the Graphene-like Sheets, *Angew. Chemie Int. Ed.* 50 (2011) 3173–3177. doi:10.1002/anie.201007520.
- [79] O. Akhavan, E. Ghaderi, S. Aghayee, Y. Fereydooni, A. Talebi, The use of a glucose-reduced graphene oxide suspension for photothermal cancer therapy, *J. Mater. Chem.* 22 (2012) 13773. doi:10.1039/c2jm31396k.
- [80] H.N. Tien, V.H. Luan, T.V. Cuong, B.-S. Kong, J.S. Chung, E.J. Kim, S.H. Hur, Fast

- and Simple Reduction of Graphene Oxide in Various Organic Solvents Using Microwave Irradiation, *J. Nanosci. Nanotechnol.* 12 (2012) 5658–5662. doi:10.1166/jnn.2012.6340.
- [81] S. Abdolhosseinzadeh, H. Asgharzadeh, S. Sadighikia, A. Khataee, UV-assisted synthesis of reduced graphene oxide–ZnO nanorod composites immobilized on Zn foil with enhanced photocatalytic performance, *Res. Chem. Intermed.* 42 (2016) 4479–4496. doi:10.1007/s11164-015-2291-z.
- [82] O. Frank, M. Mohr, J. Maultzsch, C. Thomsen, I. Riaz, R. Jalil, K.S. Novoselov, G. Tsoukleri, J. Parthenios, K. Papagelis, L. Kavan, C. Galiotis, Raman 2D-Band Splitting in Graphene: Theory and Experiment, *ACS Nano.* 5 (2011) 2231–2239. doi:10.1021/nn103493g.
- [83] M.M. Lucchese, F. Stavale, E.H.M. Ferreira, C. Vilani, M.V.O. Moutinho, R.B. Capaz, C.A. Achete, A. Jorio, Quantifying ion-induced defects and Raman relaxation length in graphene, *Carbon N. Y.* 48 (2010) 1592–1597. doi:10.1016/j.carbon.2009.12.057.
- [84] S. Stankovich, D.A. Dikin, R.D. Piner, K.A. Kohlhaas, A. Kleinhammes, Y. Jia, Y. Wu, S.T. Nguyen, R.S. Ruoff, Synthesis of graphene-based nanosheets via chemical reduction of exfoliated graphite oxide, *Carbon N. Y.* 45 (2007) 1558–1565. doi:10.1016/j.carbon.2007.02.034.
- [85] A. Ganguly, S. Sharma, P. Papakonstantinou, J. Hamilton, Probing the Thermal Deoxygenation of Graphene Oxide Using High-Resolution In Situ X-ray-Based Spectroscopies, *J. Phys. Chem. C.* 115 (2011) 17009–17019. doi:10.1021/jp203741y.
- [86] C. Chen, W. Kong, H.-M. Duan, J. Zhang, Theoretical simulation of reduction mechanism of graphene oxide in sodium hydroxide solution., *Phys. Chem. Chem. Phys.* (2014). doi:10.1039/c4cp01031k.
- [87] A.M. Dimiev, L.B. Alemany, J.M. Tour, Graphene Oxide. Origin of Acidity, Its Instability in Water, and a New Dynamic Structural Model, *ACS Nano.* 7 (2013) 576–588. doi:10.1021/nn3047378.
- [88] X. Fan, W. Peng, Y. Li, X. Li, S. Wang, G. Zhang, F. Zhang, Deoxygenation of

Exfoliated Graphite Oxide under Alkaline Conditions: A Green Route to Graphene Preparation, *Adv. Mater.* 20 (2008) 4490–4493.
doi:10.1002/adma.200801306.

- [89] Y. Matsumoto, M. Koinuma, S. Ida, S. Hayami, T. Taniguchi, K. Hatakeyama, H. Tateishi, Y. Watanabe, S. Amano, Photoreaction of Graphene Oxide Nanosheets in Water, *J. Phys. Chem. C.* 115 (2011) 19280–19286.
doi:10.1021/jp206348s.
- [90] G. He, Y. Song, K. Liu, A. Walter, S. Chen, S. Chen, Oxygen Reduction Catalyzed by Platinum Nanoparticles Supported on Graphene Quantum Dots, *ACS Catal.* 3 (2013) 831–838. doi:10.1021/cs400114s.